nature neuroscience

ARTICLES

https://doi.org/10.1038/s41593-018-0294-y

TDP-43 extracted from frontotemporal lobar degeneration subject brains displays distinct aggregate assemblies and neurotoxic effects reflecting disease progression rates

Florent Laferrière[1,13], Zuzanna Maniecka[1,13], Manuela Pérez-Berlanga[1], Marian Hruska-Plochan[1], Larissa Gilhespy[1], Eva-Maria Hock[1], Ulrich Wagner[2], Tariq Afroz[1], Paul J. Boersema[3], Gery Barmettler[4], Sandrine C. Foti[5,6], Yasmine T. Asi[5,6], Adrian M. Isaacs[6,7], Ashraf Al-Amoudi[8], Amanda Lewis[8], Henning Stahlberg[8], John Ravits[9], Francesca De Giorgi[10,11,12], François Ichas[10,11,12], Erwan Bezard[11,12], Paola Picotti[4], Tammaryn Lashley[5,6] and Magdalini Polymenidou[1*]

Accumulation of abnormally phosphorylated TDP-43 (pTDP-43) is the main pathology in affected neurons of people with amyotrophic lateral sclerosis (ALS) and frontotemporal lobar degeneration (FTLD). Morphological diversity and neuroanatomical distribution of pTDP-43 accumulations allowed classification of FTLD cases into at least four subtypes, which are correlated with clinical presentations and genetic causes. To understand the molecular basis of this heterogeneity, we developed SarkoSpin, a new method for biochemical isolation of pathological TDP-43. By combining SarkoSpin with mass spectrometry, we revealed proteins beyond TDP-43 that become abnormally insoluble in a disease subtype–specific manner. We show that pTDP-43 extracted from brain forms stable assemblies of distinct densities and morphologies that are associated with disease subtypes. Importantly, biochemically extracted pTDP-43 assemblies showed differential neurotoxicity and seeding that were correlated with disease duration of FTLD subjects. Our data are consistent with the notion that disease heterogeneity could originate from alternate pathological TDP-43 conformations, which are reminiscent of prion strains.

Amyotrophic lateral sclerosis (ALS) and frontotemporal lobar degeneration (FTLD) are devastating neurodegenerative disorders sharing genetic, neuropathological and clinical features[1]. Both diseases are characterized by pathological, ubiquitinated protein inclusions in affected neurons, which in almost all people with ALS and ~45% of people with FTLD contain the RNA-binding protein TDP-43 (ref. [2,3]). TDP-43 is a member of the heterogeneous nuclear ribonucleoprotein (hnRNP) family[4] and has essential roles in splicing regulation[5,6] that depend on the formation of physiological homo-oligomers[7–9]. TDP-43 is predominantly nuclear, but can shuttle to the cytoplasm[10], where it incorporates into stress[11] and transporting RNA[12,13] granules via its low-complexity domain, which mediates phase separation[14,15]. FTLD- and ALS-associated TDP-43 undergoes several abnormal post-translational modifications including polyubiquitination, hyperphosphorylation and proteolytic cleavage[2,3]. The latter leads to the formation of highly aggregation-prone C-terminal fragments that are deposited in inclusions along with full-length TDP-43 (refs. [16,17]).

TDP-43 neuropathology shows diverse histological patterns that are correlated with clinical presentations[18], including behavioral variant frontotemporal dementia, semantic dementia and primary nonfluent aphasia[19]. Based on morphology and neuroanatomical distribution of pathological TDP-43, FTLD-TDP can be classified into the following subtypes[20,21]. FTLD-TDP type A (FTLD-TDP-A) is characterized by neuronal cytoplasmic inclusions (NCIs), dystrophic neurites and neuronal intranuclear inclusions in upper cortical layers and typically manifests with behavioral variant frontotemporal dementia, but no motor neuron disease. Some FTLD-TDP-A subjects carry mutations in *GRN* or *C9orf72*; these cases are indistinguishable from sporadic ones. FTLD-TDP type B (FTLD-TDP-B) cases, which can also be linked to *C9orf72* mutations, show primarily granular NCIs expanding across all cortical layers, and show a combination of frontotemporal dementia and motor neuron disease. Finally, FTLD-TDP type C (FTLD-TDP-C) comprises long and thick dystrophic neurites and few NCIs, which are primarily found in superficial cortical layers. These cases are sporadic and show semantic dementia without motor neuron disease.

[1]Institute of Molecular Life Sciences, University of Zurich, Zurich, Switzerland. [2]Department of Pathology and Molecular Pathology, University Hospital Zurich, Zurich, Switzerland. [3]Institute of Biochemistry, Department of Biology, ETH Zurich (ETHZ), Zurich, Switzerland. [4]Center for Microscopy and Image Analysis, University of Zurich, Zurich, Switzerland. [5]Queen Square Brain Bank for Neurological diseases, Department of Movement Disorders, UCL Institute of Neurology, London, UK. [6]Department of Neurodegenerative Disease, UCL Institute of Neurology, London, UK. [7]UK Dementia Research Institute at UCL, UCL Institute of Neurology, London, UK. [8]Center for Cellular Imaging and NanoAnalytics (C-CINA), Biozentrum, University of Basel, Basel, Switzerland. [9]Department of Neuroscience, University of California, San Diego, La Jolla, CA, USA. [10]INSERM U1084, Laboratoire des Neurosciences Expérimentales et Cliniques, Université de Poitiers, Poitiers, France. [11]Université de Bordeaux, Institut des Maladies Neurodégénératives, UMR 5293, Bordeaux, France. [12]CNRS, Institut des Maladies Neurodégénératives, UMR 5293, Bordeaux, France. [13]These authors contributed equally: Florent Laferrière, Zuzanna Maniecka. *e-mail: magdalini.polymenidou@imls.uzh.ch

Recently, other subtypes that do not fully adhere to these pathological classification criteria have been described[20,21], suggesting that researchers are only beginning to identify the full spectrum of disease heterogeneity, whose origin remains unknown but has been proposed to be correlated with specific molecular signatures[22,23].

To address the molecular underpinnings of disease heterogeneity, we sought to analyze the biochemical characteristics of TDP-43 aggregates, which requires their physical separation from physiological TDP-43 and other proteins. We developed SarkoSpin, a new, simple method for pathological TDP-43 extraction. Using SarkoSpin on brain cortical samples from >80 subjects, we found that TDP-43 forms large assemblies of distinct densities, polyubiquitination levels and morphologies that are correlated with specific neuropathological classifications. Coupling SarkoSpin with mass spectrometry, we identified a subset of insoluble proteins beyond TDP-43 in each disease subtype. These proteins rarely co-aggregate with pTDP-43 and probably represent a downstream effect of TDP-43 pathology. Importantly, we show that SarkoSpin-extracted pTDP-43 assemblies exhibit cytotoxicity and protein seeding with potency that reflects the disease duration of the respective subtype. Collectively, our data demonstrate that FTLD heterogeneity is reflected in the biochemical, neurotoxic and seeding properties of TDP-43. We propose that alternative TDP-43 pathological conformations may underlie the diversity of TDP-43 proteinopathies, in a manner reminiscent of prion strains[24,25].

Results

Subject cohort and characterization of FTLD-TDP cases. Brain cortical samples from >80 subjects, including control subjects with no apparent central nervous system pathology or with non-TDP-43-linked neurodegeneration, as well as ALS and FTLD subjects of different subtypes were obtained from three different centers worldwide (Supplementary Table 1). The morphology and neuroanatomical distribution of pathological TDP-43 accumulations of these cases (Supplementary Fig. 1a) adhered to the current classifications[20,21]. FTLD-TDP-C subjects in our cohort showed significantly longer disease duration compared to all other subtypes (Supplementary Fig. 1b,c), in agreement with a recent report[21].

SarkoSpin isolates pathological TDP-43 from human brain. Although pathological TDP-43 is resistant to detergents such as sarkosyl[22,26–28], there is currently no method that allows the physical separation of pathological TDP-43 from the protein pool in complex tissues. Instead, physiological TDP-43, as well as other proteins containing low-complexity domains, typically co-purify with pathological TDP-43 in sarkosyl-insoluble fractions from subject brain tissue[27,28] (Supplementary Fig. 2a,b). This contamination is probably due to the formation of large complexes with nucleic acids, including physiological nuclear TDP-43 oligomers[7], which become partially resistant to detergent solubilization (Supplementary Fig. 2b).

To overcome this limitation and to purify pathological TDP-43 from its normal counterpart, we combined harsh solubilization with nuclease treatment and a single centrifugation step in a new method we termed SarkoSpin (Fig. 1a,b). To assess the efficiency of our technique, we analyzed motor and frontal cortex homogenates from control, ALS and FTLD-TDP subjects (Supplementary Table 1). Total protein amounts partitioning in the SarkoSpin supernatant and pellet fractions were estimated by silver staining of SDS–polyacrylamide gel electrophoresis (SDS–PAGE)-analyzed samples (Fig. 1c and Supplementary Fig. 2c) and by measuring protein concentrations. On average, 99.8% of the total protein mass resided in the supernatant with no significant difference among groups (Fig. 1d). Some 99.9% of total TDP-43 was found in the supernatants of control samples (Fig. 1e,f and Supplementary Fig. 3), whereas in disease cases this was only 88%, indicating that the rest of TDP-43 was present in the sarkosyl-insoluble pellet, corresponding to the pathological species. Indeed, the pellet fraction showed the characteristic signature for pathological TDP-43 (namely polyubiquitination, C-terminal cleavage and hyperphosphorylation), which was detected by antibodies to total TDP-43 or phosphorylated TDP-43 (pSer409 or pSer410) (Fig. 1b,e,f and Supplementary Fig. 3). The latter showed 64% enrichment in disease pellets with no significant difference between disease types (Fig. 1g,h). Proteins with low-complexity domains or RNA- and DNA-binding ability, such as other members of the hnRNP family, as well as other ALS- or frontotemporal dementia–associated proteins (FUS, hnRNPA1, hnRNPH and SOD1) and normal proteins partitioning in complex macromolecular assemblies (actin and histones), were undetectable in SarkoSpin pellets (Fig. 1i,j and Supplementary Fig. 3).

SarkoSpin captures native pathological TDP-43 assemblies. To further characterize the properties of these assemblies, we next performed native PAGE of SarkoSpin samples. Supernatants of all cases including controls showed a wide smear, ranging from the stacking gel (>10 MDa) to the size of monomeric TDP-43, where a strong band was observed (Supplementary Fig. 4a), suggesting that TDP-43 occurs in different oligomeric states, in agreement with our recent report[7]. Notably, total protein concentrations were equalized before SarkoSpin, explaining the lower signal observed in controls, which lack TDP-43 aggregates. Notably, a strong TDP-43 signal, which was also detectable with an antibody to pTDP-43, was observed in the stacking gel in subject, but not in control samples (Supplementary Fig. 4b), corresponding to the pathological species. Importantly, in contrast to control samples, SarkoSpin-pelleted ALS and FTLD samples immunoblotted with antibodies to total TDP-43 or pTDP-43 revealed solely the presence of high-molecular-mass assemblies retained in the stacking gels (Supplementary Fig. 4c,d), further confirming the efficient separation of pathological from physiological assemblies. If such high-ordered aggregates were exclusively composed of TDP-43, they would consist of at least 200 monomers, which may represent the minimal unit comprising the large inclusions found in ALS- and FTLD-affected neurons. Although we observed no differences among the various disease types, we cannot exclude the possibility that subtype-specific differences undetectable by the resolution of this assay occur above the resolved sizes.

Insoluble proteome distinguishes disease subtypes. To explore which proteins other than TDP-43 become insoluble in ALS and FTLD samples, we analyzed SarkoSpin preparations from brain homogenates of 11 controls and 27 subjects by liquid chromatography–mass spectrometry. After denaturation and normalization of protein concentrations, SarkoSpin pellets were subjected to enzymatic digestion. Tandem mass spectra acquired by high-resolution mass spectrometers were searched for in a human protein database. Spectral counting was used for quantifying differences in protein abundance between samples. The most significantly enriched protein ($P=10^{-3}$) that was most consistently correlated ($r=0.65$) with FTLD-TDP, but not with control or FTLD-Tau SarkoSpin pellets, was TDP-43 (Supplementary Fig. 5). All remaining proteins had weaker correlation values ($r<0.5$) and were less consistently enriched in the subject group, illustrating that TDP-43 is the main component of insoluble protein aggregates[2,3] and further validating SarkoSpin as a reliable method for their isolation.

Importantly, when we compared the insoluble proteins enriched in each disease group separately (Supplementary Figs. 6–9), we found that a distinct set of proteins characterized each subtype (Fig. 2a). This suggests that although TDP-43 is the only protein consistently aggregating in disease, a specific subclass of proteins accompany TDP-43 within the insoluble fraction of each disease group.

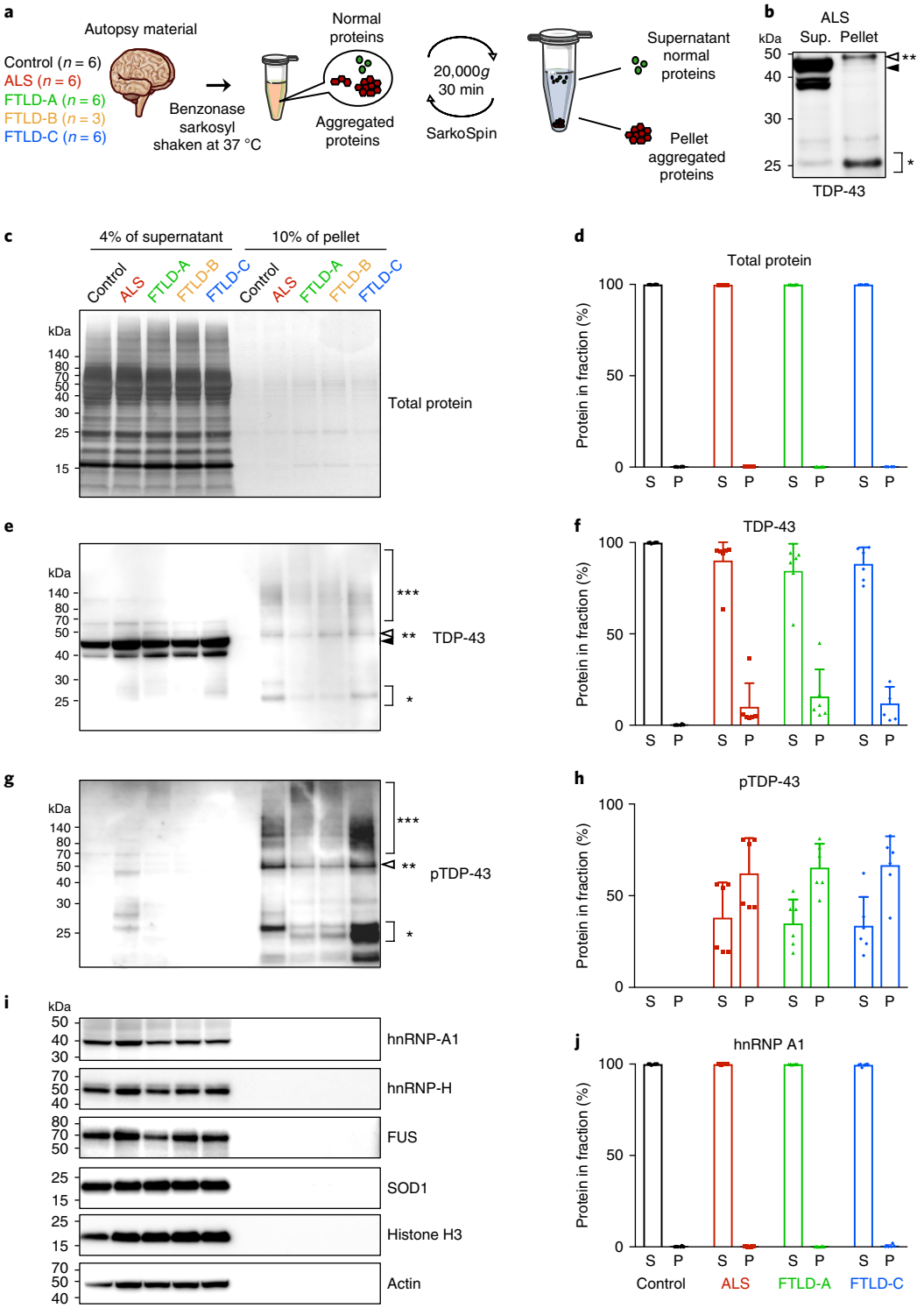

Fig. 1 | SarkoSpin physically separates pathological TDP-43 from the majority of normal proteins in FTLD and ALS brains. a, Schematic of SarkoSpin protocol, including number of autopsy samples from each disease type used in this figure. Samples were homogenized and solubilized with sarkosyl at 37 °C in presence of Benzonase before a single centrifugation step to separate supernatant and pellet fractions. **b–j**, Biochemical analysis of SarkoSpin fractions extracted from human brain samples. Supernatants and pellets were subjected to SDS–PAGE followed by silver staining of total protein (**c**), or were immunoblotted against total TDP-43 (**b**,**e**), phosphorylated TDP-43 at position Ser409 or Ser410 (pTDP-43) (**g**), or hnRNPA1, hnRNPH, FUS, SOD1, histone H3 or actin (**i**). Physiological TDP-43 was found exclusively in supernatants for all subjects, whereas the pathological species marked by phosphorylation were pelleted for all disease types but were absent in controls. Pathological post-translational modifications of TDP-43 were observed specifically in SarkoSpin pellets of disease cases: polyubiquitination smear (***), hyperphosphorylation of TDP-43 detected by both anti-pTDP-43 (Ser409 or Ser410) and anti-TDP-43 (total) as a slower migrating band at 45 kDa (**) and at the C-terminal fragment of 25 kDa (*). **d**,**f**,**h**,**j**, Quantification of the percentage of each protein residing in SarkoSpin supernatant or pellet for all subjects used in this experiment. S, supernatant; P, pellet. Bars represent mean with s.d. $n = 6$ biologically independent human brain samples for control, ALS, FTLD-TDP-A and FTLD-TDP-C groups. The results shown in **b**,**c**,**e**,**g**,**i** were repeated twice with all 27 independent biological samples with similar results; quantifications of one experiment are shown in **d**,**f**,**h**,**j**.

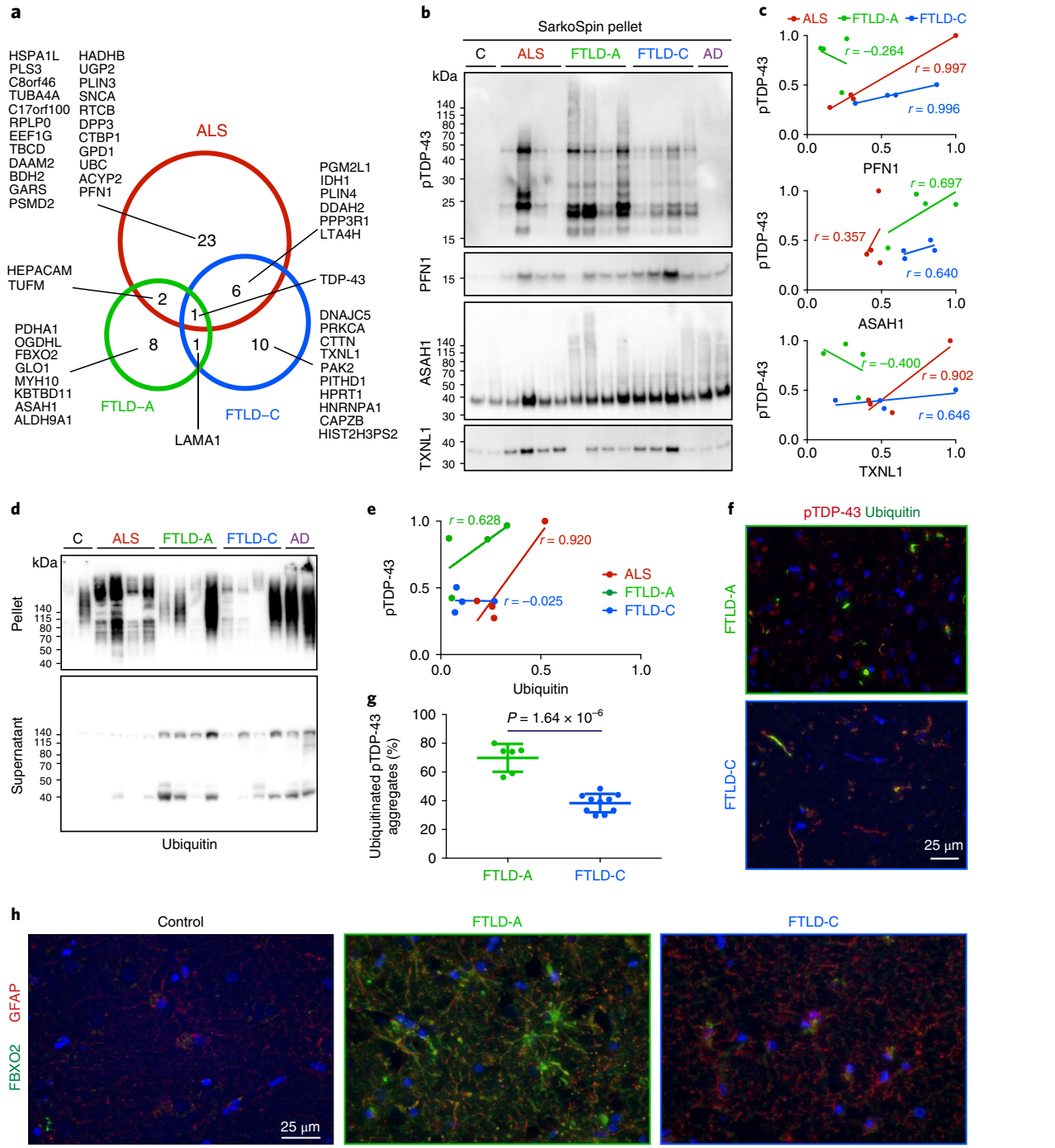

Fig. 2 | SarkoSpin extracts from different disease subtypes have distinct protein compositions beyond TDP-43. a, Overlap of proteins with the highest values of idealized vector correlation when comparing each ALS, FTLD-TDP-A and FTLD-TDP-C sample to controls (Pearson's correlation method). Only proteins with correlation values >0.5 were taken into account. Proteins further validated by immunoblot and immunohistochemistry are in bold. **b**, Representative immunoblots on SarkoSpin pellets probed against several mass spectrometry hits (PFN1, ASAH1 and TXNL1), showing their enrichment in the insoluble fraction in respective disease subtypes. C, control; AD; Alzheimer's disease. **c**, Correlation dot plots of pTDP-43 levels and insolubility of selected mass spectrometry candidates analyzed in **b** (Pearson's correlation method). **d**, Representative immunoblots on SarkoSpin pellet and supernatant fractions probed with ubiquitin antibody, indicating enrichment of ubiquitinated pathological assemblies in SarkoSpin pellet fractions. **e**, Correlation dot plot of pTDP-43 and ubiquitin levels in SarkoSpin pellets across disease subtypes (Pearson's correlation method). **f**, Co-immunofluorescence of pTDP-43 with ubiquitin in FTLD-TDP-A and FTLD-TDP-C postmortem brain sections. **g**, Quantification of aggregates double-positive for pTDP-43 and ubiquitin in FTLD-TDP-A and FTLD-TDP-C (dots represent single percentage values quantified per each image; error bars show mean with s.d., unpaired two-sided *t* test with $P = 1.64 \times 10^{-6}$). **h**. Representative images of co-immunofluorescence of GFAP marking astrocytes with a mass spectrometry hit FBXO2. In panels **f**,**h**, images are overlaid with DAPI nuclear staining in blue. For **c**,**e**,**g**, $n = 4$ biologically independent human brain samples for ALS, FTLD-TDP-A and FTLD-TDP-C groups. In **b**,**d**,**f**,**h**, results were repeated twice independently for all $n = 4$ independent biological samples of each disease group with similar results.

To confirm these findings, we first tested several commercially available antibodies for sensitivity and specificity to proteins predicted to be correlated with pTDP-43 levels in specific disease subtypes (Fig. 2a). Based on the antibodies' performance, we selected one protein per disease group, namely profilin 1 (PFN1), which is enriched in ALS cases and reported to be mutated in rare familial ALS cases[29,30], *N*-acylsphingosine amidohydrolase (ASAH1), which is enriched in FTLD-TDP-A cases and mutated in some cases of spinal muscular atrophy[31,] and thioredoxin-like protein 1 (TXNL1), which is enriched in FTLD-TDP-C in our data set. We then tested the presence of these proteins in SarkoSpin fractions of individual subjects by immunoblot and found that, although their levels on SarkoSpin supernatants were comparable (Supplementary Fig. 10a,b), they were enriched in the pellets of samples from TDP-43 proteinopathies (Fig. 2b). Notably, this enrichment was best correlated with pTDP-43 levels in the respective disease subtype (Fig. 2c), in agreement with our mass spectrometry results. Despite the large variability in pTDP-43 levels of individual subject samples, we confirmed the validity of these correlations by the almost perfect correlation for all groups with total TDP-43 in these pellets (Supplementary Fig. 10c,d).

A similar approach was used to examine the correlation of ubiquitin and pTDP-43 levels in SarkoSpin pellets, leading to an observation we did not expect. Ubiquitin blots of SarkoSpin pellets and supernatants showed completely different patterns, with ubiquitin-positive smears characteristic for pathological polyubiquitination present only in the pellets (Fig. 2d), confirming that SarkoSpin specifically concentrated misfolded proteins that escape proteasome degradation. To our surprise, ubiquitin levels of pTDP-43 extracted from FTLD-TDP-C subjects were consistently lower than those derived from FTLD-TDP-A and ALS subjects (Fig. 2d,e). Comparison of co-immunofluorescence analysis of pTDP-43 and ubiquitin on subject brain sections confirmed the differential levels of pTDP-43 polyubiquitination (Fig. 2f,g and Supplementary Fig. 10e).

With the exception of a few identified proteins such as LAMA1 and HepaCAM, which belong to the extracellular matrix and probably associate with TDP-43 after tissue lysis, all proteins found in subject SarkoSpin pellets were localized intracellularly. To investigate whether the increased insolubility of ASAH1 and TXNL1 resulted from direct co-aggregation with pTDP-43, or whether these proteins become insoluble as a consequence of TDP-43 aggregation, similar to findings in other proteinopathies[32], we performed co-immunofluorescence analysis with pTDP-43 on brain sections. ASAH1 and TXNL1 both demonstrated cytoplasmic staining, which was increased and displayed a punctate pattern in both subject subtypes (Supplementary Fig. 11). This pattern seemed largely independent of pTDP-43 inclusions, with rare colocalization observable in both disease subtypes. This suggested that increased insolubility of these proteins in disease does not result from direct interaction and co-aggregation with pTDP-43 and that SarkoSpin probably dissociated other proteins that co-aggregate with pTDP-43 on subject tissues[33], thereby releasing the pTDP-43 'core' of these pathological assemblies.

Importantly, one of the proteins enriched in FTLD-TDP-A in our mass spectroscopy analysis was the F-box protein 2 (FBXO2), which during our initial screen by conventional immunohistochemistry stained neuronal cytoplasm in control and FTLD-TDP-C brain sections; in contrast, a characteristic astrocytic-like pattern was observed in the FTLD-TDP-A subtype (Supplementary Fig. 12a). To further explore this finding, we performed co-immunofluorescence analysis of FBXO2 and the astrocytic marker glial fibrillary acidic protein (GFAP). Notably, although astrogliosis was evident through increased GFAP staining in both disease subtypes, FBXO2 marked FTLD-TDP-A but not FTLD-TDP-C astrocytes (Fig. 2h and Supplementary Fig. 12b). These data indicate a previously unrecognized distinct astrocytic reaction characterizing FTLD-TDP-A subjects, illustrating divergent pathogenic mechanisms within these two disease subtypes.

Diverse TDP-43 aggregate sizes in different disease subtypes. We next assessed the sedimentation profiles of TDP-43 aggregates to uncover specific size or shape differences among disease subtypes. Brain cortex homogenates of eight controls and 27 subjects were SarkoSpin-solubilized and layered on top of linearized iodixanol gradients before ultracentrifugation (Fig. 3a). Gradients were fractionated in 16 fractions of equal volume, and TDP-43 or pTDP-43 distribution was assessed by immunoblotting. In both control and disease samples, monomeric and oligomeric TDP-43 were retained in the top five fractions, peaking in the first three (Fig. 3b–d and Supplementary Figs. 13 and 14a,b). In addition, populations of larger sizes carrying the specific post-translational modifications of pathological TDP-43 were identified specifically in disease cases. In ALS samples, sedimentation profiles revealed one population of aggregated and phosphorylated TDP-43 in fractions 8–13 and peaking between fractions 10 and 11. FTLD-TDP-A sedimentations revealed a wide diversity of profiles, with TDP-43 aggregates sedimenting in fractions 5–14, and two apparent populations peaking in fractions 6–7 and in fraction 11. The presence of a second subpopulation could indicate a difference in size or shape of the aggregates. Notably, neuropathological type rather than *C9orf72* mutation was better correlated with the size distribution of TDP-43 aggregates, as they followed the pattern observed for the respective disease type (peaks in fractions 6–7 and 11 for type A and in fractions 10–12 for type B) and clearly separated into different groups. FTLD-TDP-C sedimentation profiles also revealed one broad population of TDP-43 aggregates (Fig. 3b,c and Supplementary Figs. 13 and 14a,b). However, in contrast to the other types, these assemblies sedimented further in fractions 10–16, which may reflect their bigger size and/or higher intrinsic density. Importantly, hnRNPA1, FUS and SOD1 remained in the first three fractions in all disease types and controls (Supplementary Fig. 14c), indicating that solubility of these proteins is not significantly altered in TDP-43 proteinopathies.

TDP-43 aggregate densities distinguish disease subtypes. To determine whether the observed differences in velocity sedimentation were due to distinct aggregate size, shape or density, we sought to measure the intrinsic density of TDP-43 aggregates. To this end, we submitted the same subject samples to SarkoSpin solubilization, followed by ultracentrifugation in an iodixanol discontinuous gradient for 17 h to reach isopycnic equilibrium[24] (Fig. 4a). Gradients were then fractionated, and TDP-43 and pTDP-43 density profiles were determined as described above (Fig. 4b–d and Supplementary Figs. 15 and 16a,b).

In all samples, the majority of normal TDP-43 was present in one peak spanning fractions 8–12, at an average density of 1.22 g ml^{-1}. Notably, all density gradients from ALS, FTLD-TDP-A (Fig. 4b,c) and FTLD-TDP-B cases (Supplementary Fig. 15a) showed an additional population of TDP-43, present in one sharp peak in fraction 7, corresponding to density of 1.16 g ml^{-1}. This consistent population showed all known TDP-43 pathological features, namely ubiquitination, C-terminal cleavage and phosphorylation (Supplementary Fig. 16a,b). To our surprise, density profiles of all nine FTLD-TDP-C samples were significantly different from all other types of TDP-43 proteinopathies tested, with a peak of pTDP-43 intermingling with the normal TDP-43 peak in fractions 8–10, at a density of 1.20 g ml^{-1} (Fig. 4b,c and Supplementary Figs. 15b and 16b).

We next performed native-PAGE immunoblots on density floatation gradient fractions. Two major populations were distinguishable in all cases, including controls: one in fractions 8–12 under 66 kDa, and one in fractions 5–7 smearing from 66 kDa to 10 MDa. The latter represented TDP-43 oligomers[7], which were more

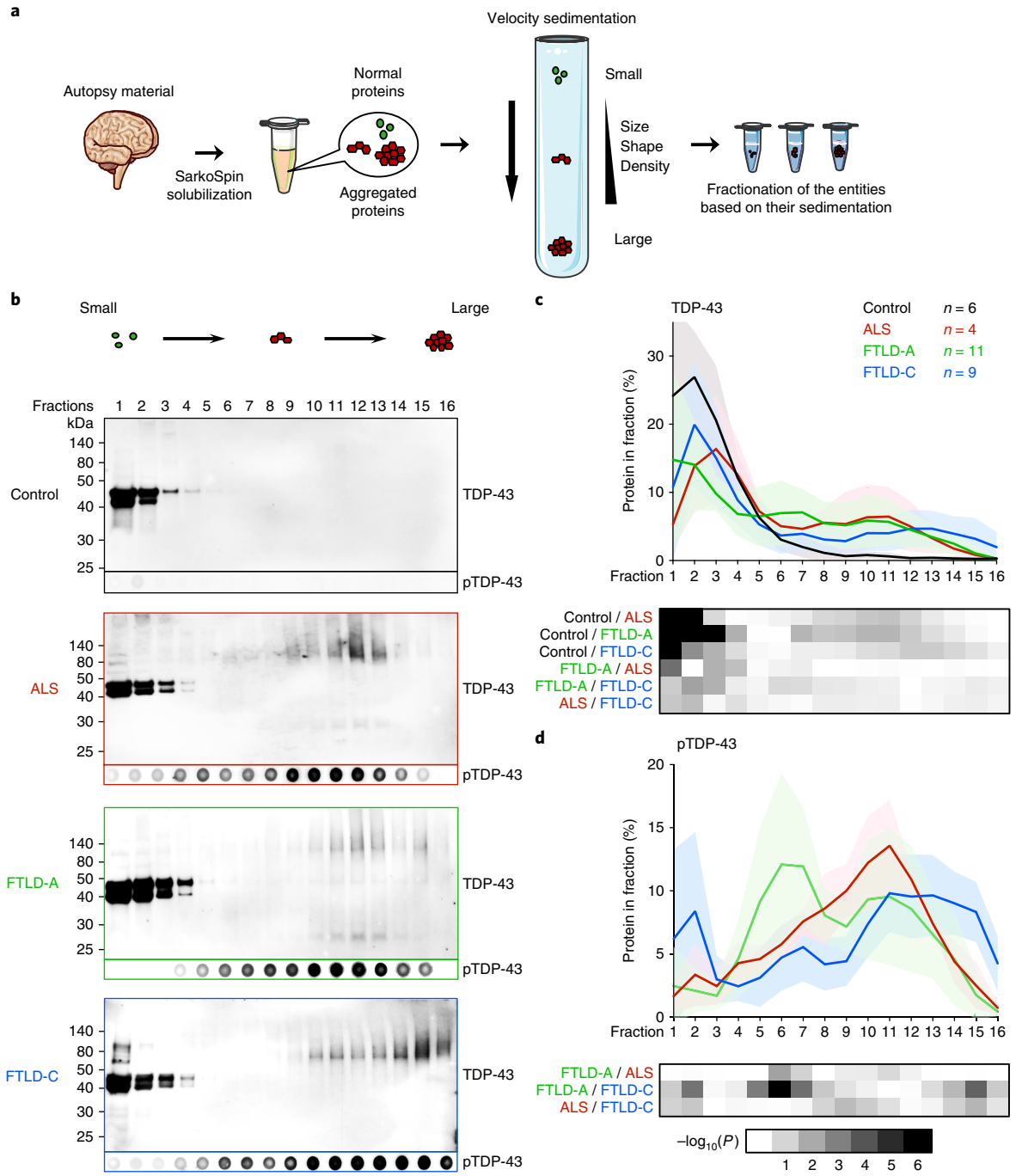

Fig. 3 | Diverse size distributions of TDP-43 aggregates isolated from different types of TDP-43 proteinopathies. a, Schematic representation of the velocity sedimentation protocol. After SarkoSpin solubilization, brain homogenates were loaded on top of iodixanol gradients and fractionated by sedimentation velocity upon ultracentrifugation. **b**, Representative immunoblots of the velocity sedimentation profiles of physiological and pathological TDP-43 in various disease types. SarkoSpin-solubilized brain homogenates from frontal and motor cortex of control (black), ALS (red), FTLD-TDP-A (green) and FTLD-TDP-C (blue) brains were fractionated by velocity sedimentation and the distribution of total TDP-43 (top, immunoblots) and of pTDP-43 (bottom, dot blots) was analyzed in the collected fractions (numbered from top to bottom of gradient). Immunoblots were repeated three times independently with similar results. **c**,**d**, The relative amounts of TDP-43 (**c**), and pTDP-43 (**d**) per fraction were quantified from control (black, $n=6$), ALS (red, $n=4$), FTLD-TDP A (green, $n=10$), FTLD-TDP C (blue, $n=8$) velocity sedimentation fractionations, with n being the number of biologically independent human brain samples. Data presented are the mean curves (bold lines) with s.d. (lighter shaded areas) for each subject group. Panels below the graphs show the statistical significance of the difference in TDP-43 partition in each fraction, based on two-way ANOVA followed by Tukey's multiple-comparison tests.

buoyant than monomeric species and comprised an estimated 25–35% of total TDP-43 in controls. Importantly, in agreement with Fig. 4, the high-molecular-mass pTDP-43 aggregates were present in fractions 7 and 8–10 for FTLD-TDP-A and FTLD-TDP-C, respectively (Supplementary Fig. 16c). Collectively, these results show that pathological TDP-43 aggregates extracted from FTLD-TDP-C were ordered in a different fashion than those found in other FTLD-TDP subtypes or ALS.

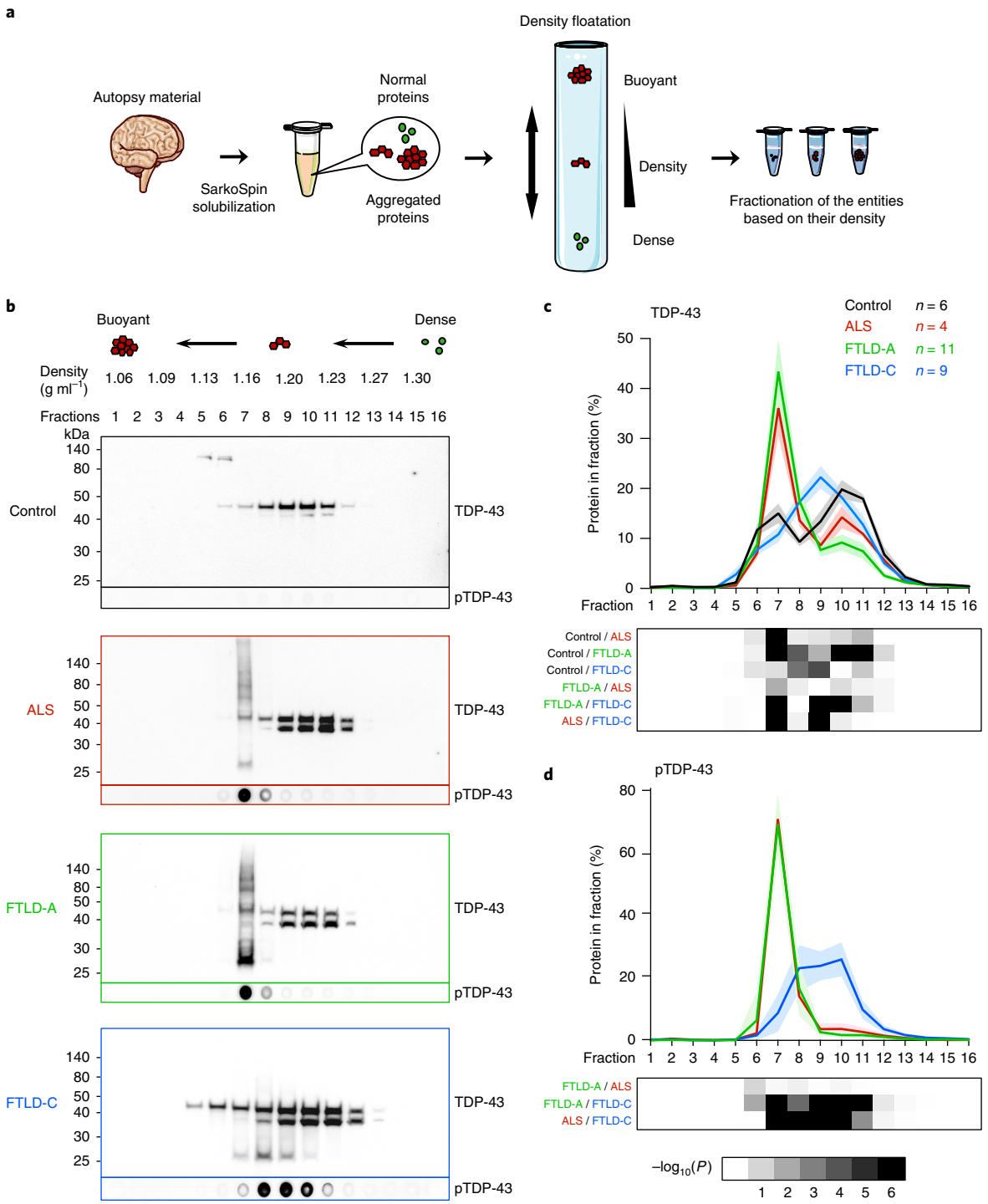

Fig. 4 | Distinct density profiles of TDP-43 aggregates isolated from different types of TDP-43 proteinopathies. a, Schematic of the density floatation protocol. Briefly, after SarkoSpin solubilization, brain homogenates were loaded in the middle of iodixanol gradients and fractionated by density upon isopycnic equilibrium ultracentrifugation. **b**, Representative immunoblots of the density sedimentation profiles of physiological and pathological TDP-43 in various disease types. SarkoSpin-solubilized brain homogenates from frontal and motor cortex of control (black), ALS (red), FTLD-TDP-A (green) and FTLD-TDP-C (blue) samples were fractionated by density and the distribution of total TDP-43 (top, immunoblots) and of pTDP-43 (bottom, dot blots) was analyzed in the collected fractions (numbered from top to bottom of the gradient). Density values calculated by refractometry are indicated on top of graph. Immunoblots were repeated three times independently with similar results. **c**,**d**, Relative amounts of TDP-43 (**c**) and pTDP-43 (**d**) per fraction were quantified from all immunoblots of control (black, $n=6$), ALS (red, $n=4$), FTLD-TDP-A (green, $n=10$), FTLD-TDP-C (blue, $n=8$) density fractionations, with n being the number of biologically independent human brain samples. Data presented are mean curves (bold lines) with s.d. (lighter shaded areas) for each group of subjects. Panels below graphs show statistical significance of difference in TDP-43 partition in each fraction based on two-way ANOVA followed by Tukey's multiple-comparison tests.

Alternate TDP-43 aggregate morphologies in disease subtypes. To visualize TDP-43 aggregates, anti-TDP-43 immunogold labeling followed by transmission electron microscopy (TEM) was performed on SarkoSpin pellets. To avoid drying artifacts, samples were embedded in methylcellulose. No immunoreactivity or large protein assemblies were detected in control samples. In contrast, FTLD-TDP-A and FTLD-TDP-C SarkoSpin pellets contained many protein structures of various shapes and sizes, ranging from 50 to 150 nm, and decorated by gold bead–labeled antibody to TDP-43 (Fig. 5a, red arrows). Notably, although the same monoclonal antibody recognizing a short epitope spanning amino acids 203–209 did not show consistent differences between the two disease groups under denaturing conditions, immunogold electron microscopy (immunogold-EM) revealed differential immunoreactivity, with strongly immunopositive FTLD-TDP-A assemblies and only sparsely labeled FTLD-TDP-C aggregates. This lower antibody detection indicates distinct epitope accessibility, and thus different packaging of pathological TDP-43 type A versus type C aggregates. It is conceivable that the antibody epitope, which lies within the second RNA recognition motif (RRM2), is buried inside the core of FTLD-TDP-C aggregates. These results corroborate the higher density of type C aggregates and their discriminating three-dimensional shapes compared to type A aggregates.

Notably, we did not detect any long amyloid fibrils in any disease case, in agreement with the apparent lack of amyloidophilic staining in the majority of ALS and FTLD subject brains[34,35]. Nevertheless, careful observation of the immunogold-EM images suggested the presence of short proteinaceous filaments, which were 5–8 nm thick and 30–50 nm long and were frequently decorated by the antibody to TDP-43 in FTLD-TDP-A (Fig. 5a, orange arrows). Similar structures were detected in FTLD-TDP-C samples, albeit mostly independently from antibody labeling (Fig. 5b, orange arrows). These structures potentially originated from filamentous material in FTLD brains, as previously reported[36], which is in agreement with a recent study showing a high-resolution structure of a short TDP-43 low-complexity domain–derived peptide[37].

As the use of methylcellulose lowers image resolution, immunolabeled SarkoSpin pellets prepared without this preservation step were also analyzed by TEM. This allowed us to obtain higher-resolution images of type A TDP-43 aggregates. These showed heterogeneous spheroid or elongated and coiled protein assemblies (Fig. 5c). Owing to lower immunoreactivity, such structures could not be identified in FTLD-TDP-C samples. Importantly, neither method for immunogold-labeled sample preparation showed nonspecific binding of the gold-conjugated secondary antibody (Supplementary Fig. 17a). Lipids, which sometimes appeared adjacent to TDP-43 aggregates (Fig. 5a, yellow arrows), could be removed by a slight adaptation of the SarkoSpin method with centrifugation over a sucrose cushion (Supplementary Fig. 17b).

To obtain an independent, albeit indirect, measure of the different conformational features of TDP-43 aggregates, we used partial proteolysis. This method has been used extensively as a surrogate for probing different pathological conformations of the prion protein, because the proteolytic fragment size is directly related to site accessibility to proteases[25,38]. In contrast to the prion protein, TDP-43 is largely sensitive to proteinase K (Supplementary Fig. 17c), but has previously been reported to be partially resistant to chymotrypsin and trypsin[22,23]. Here, we systematically analyzed the proteolytic profile of TDP-43 species extracted from different disease subtypes (Fig. 5d). Indeed, chymotrypsin- and trypsin-treated SarkoSpin pellets showed specific and consistent proteolytic profiles in each disease subtype, suggesting that aggregate arrangement and, by extension, the borders of the protease-resistant cores are distinctive. Additionally, probing with antibodies to defined TDP-43 domains revealed resistance of the most C-terminal fragment within the low-complexity domain, suggesting that the cleavage site is hidden within the aggregate core. Notably, these fragments were significantly more resistant to proteolysis by trypsin in FTLD-TDP-C compared to FTLD-TDP-A (Fig. 5e).

Lastly, we explored this proteolytic resistance of TDP-43 species to visualize the resistant cores of the aggregates, which we identified using immunogold labeling with an antibody to the TDP-43 phosphorylation sites at amino acids 409 or 410 (Fig. 5f). This treatment led to protein structures with high anti-pTDP-43 immunopositivity for both FTLD-TDP-A and FTLD-TDP-C, further confirming that the lack of anti-RRM2 immunogold labeling in FTLD-TDP-C samples (Fig. 5a) was due to epitope accessibility within TDP-43 assemblies.

Distinct TDP-43 aggregate neurotoxicities in disease subtypes. To determine whether these distinct TDP-43 conformations were associated with different toxic properties, we tested their effect on the viability of cell lines and primary neurons. To this end, we used the Flp-In T-Rex technology to generate a stable cell line with inducible expression of C-terminally tagged TDP-43 and obtained a homogeneous population of cells expressing traceable TDP-43 at similar levels (Supplementary Fig. 18a–c). We used the nine-residue hemagglutinin (HA) tag, which we placed at the very end of the structurally disordered region to minimize any interference with protein structure, which might hinder protein seeding. We first used our TDP-43-HA-expressing cells to optimize internalization of SarkoSpin-extracted green fluorescent protein (GFP)-labeled pTDP-43 aggregates produced in cells, demonstrating that our extraction method can also be applied to cellular models of disease (Supplementary Fig. 18d–f).

To test whether SarkoSpin specifically concentrated toxic TDP-43 seeds, we subsequently introduced pellets from control and FTLD subjects into mitotically arrested cells, because continuous proliferation and high metabolic activity of these cells could mask the toxicity of exogenous aggregates. We reasoned that if toxicity of pTDP-43 assemblies depended on seeding, the effect would be more profound upon increased expression of the substrate, that is, TDP-43-HA. We therefore calculated the viability ratio of cells with or without TDP-43-HA expression and found that upon a three-fold increase in TDP-43 protein levels (Supplementary Fig. 18g), cell viability was significantly lower after inoculation with FTLD-TDP-A extracts in comparison to inoculation with control or FTLD-TDP-C aggregates (Fig. 6a,b).

To directly test whether the observed toxicity depends on aggregation of endogenous TDP-43, we subsequently performed SarkoSpin on mitotically arrested TDP-43-HA-expressing cells inoculated with SarkoSpin pellet pools from control and FTLD subjects. Immunoblot with antibody to HA against the endogenously expressed TDP-43-HA allowed for the unambiguous distinction of newly induced aggregates from exogenous subject-derived seeds. Although levels of TDP-43-HA were equal in all conditions (Supplementary Fig. 18g), cells inoculated with FTLD-TDP-A pellets showed greater TDP-43-HA aggregation compared to cells treated with control or FTLD-TDP-C seeds (Fig. 6c). Collectively, these data indicate that pTDP-43 assemblies extracted from FTLD-TDP-A, but not from control or FTLD-TDP-C subjects, were cytotoxic and induced endogenous TDP-43 aggregation, potentially via protein seeding.

To confirm the increased potency of FTLD-TDP-A aggregates in a disease-relevant system, we quantified their effect on neurite length of primary cortical neurons prepared from mouse embryos using high-content screening[39]. Neurite length is decreased by treatment with artificial oligomers of α-synuclein, which can enter cells and act as seeds of an autonucleation process[40]. Neuronal cultures were exposed to four different doses of SarkoSpin pellet pools from control, FTLD-TDP-A or FTLD-TDP-C subjects (Fig. 6d–h).

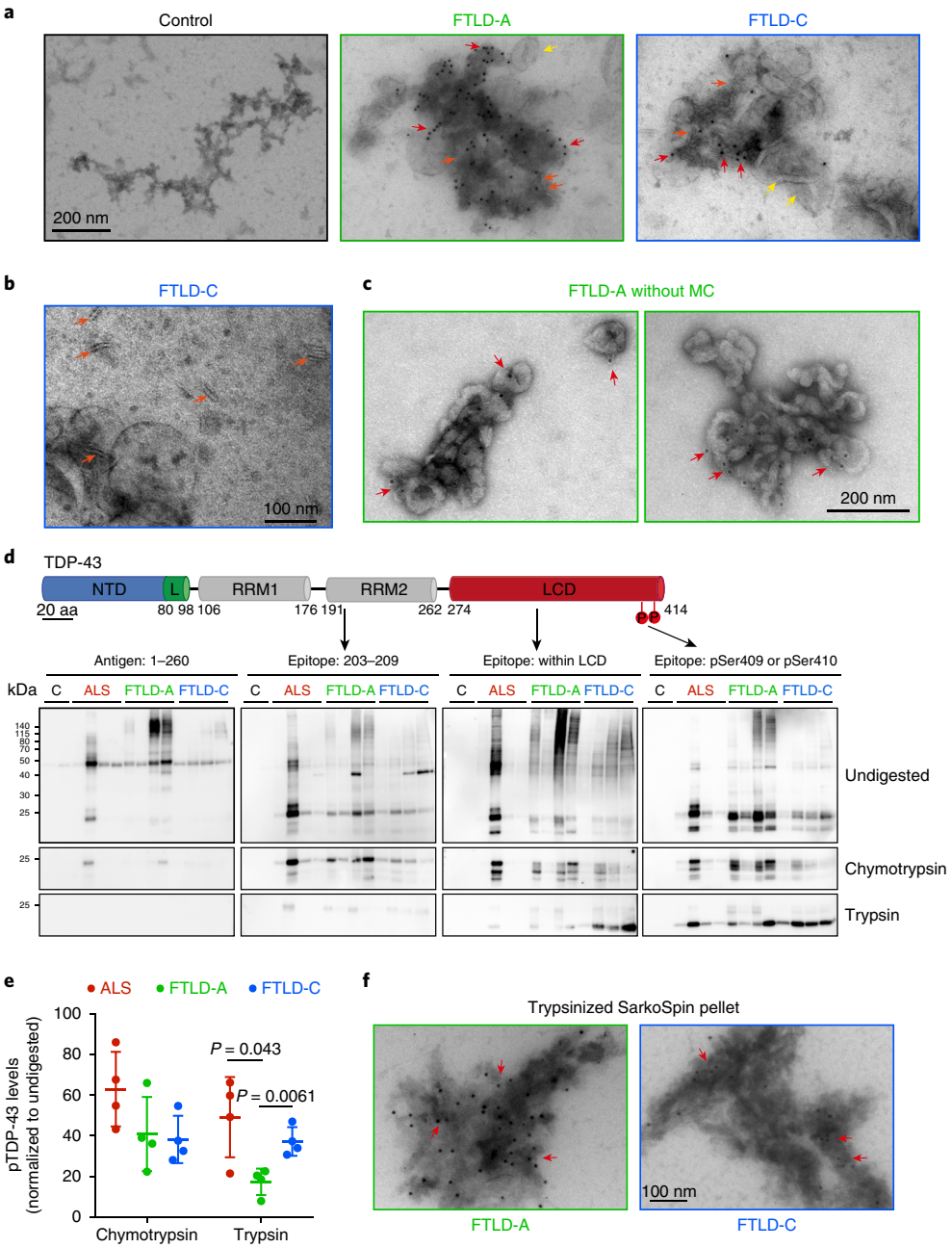

Fig. 5 | Distinct structure of pathological TDP-43 isolated from different disease subtypes. a, TEM images of SarkoSpin-extracted aggregates from control (black), FTLD-TDP type A (green) and FTLD-TDP type C (blue) samples immunolabeled with monoclonal TDP-43 antibody (epitope: 203–209). Red arrows point to gold-positive structures, yellow arrows to lipid contaminants and orange arrows to proteinaceous filamentous structures. **b**, Part of the FTLD-TDP-C image in **a** was bandpass filtered. Scale bar, 100 nm. **c**, TEM images of SarkoSpin-extracted aggregates from FTLD-TDP-A subject immunogold-labeled against TDP-43, without embedding in methylcellulose (MC). **d**, Proteolytic profiles of pathological TDP-43 from different disease subtypes as annotated. Two control samples and four disease samples were incubated with either 10 μg ml^{-1} chymotrypsin or 100 μg ml^{-1} trypsin for 30 min at 37 °C during SarkoSpin solubilization. Pellets were immunoblotted with antibodies to TDP-43. As a reference to antigens and epitopes of used antibodies, TDP-43 secondary structure is represented below. NTD, N-terminal domain; NLS, nuclear localization signal; RRM1 and RRM2, RNA-recognition motifs; LCD, low-complexity domain; phosphorylation is marked at the very C terminus; aa, amino acid. **e**, Dot plot representing levels of pTDP-43 chymotrypsin- and trypsin-resistant fragments normalized to total level of undigested TDP-43 species across disease subtypes. $n = 4$ biologically independent human brain samples per disease group and per protease used. Dots represent single analyzed subjects per disease subtype; error bars show mean with s.d. (unpaired two-sided t tests). **f**, Representative TEM images of trypsinized SarkoSpin-extracted aggregates from FTLD-TDP type A and type C immunogold-labeled against pTDP-43 pSer409 or pSer410. Red arrows point to gold-positive structures. Experiments were repeated two (**d**), three (**c**,**f**) and four (**a**,**b**) independent times with similar results.

As expected, TDP-43 and pTDP-43 were absent from control SarkoSpin pellets, whereas their quantity in FTLD-TDP-C inocula was about half that of FTLD-TDP-A for all doses (Supplementary Fig. 18i). Importantly, pTDP-43 levels were equivalent between FTLD-TDP-A at a dose of 0.3 μg and FTLD-TDP-C at 1 μg total protein, allowing direct comparison of the two types of pathological

pTDP-43 assemblies. The effect of exogenous pTDP-43 SarkoSpin extracts on neurite growth was then monitored by automated live-cell imaging with combined phase-contrast and epifluorescence imaging over 10 days (Fig. 6e,f). In line with our observations in immortalized cells, TDP-43 aggregates extracted from FTLD-TDP-A drastically reduced neurite length (Fig. 6h), which reached a plateau immediately after inoculation (after 5 days in vitro (DIV)), whereas control or FTLD-TDP-C SarkoSpin pellets had no effect. At 10 DIV, all primary neuronal cultures were submitted to calcein fluorescence imaging, allowing cell body counting and measurement of neurite length (Fig. 6g,h). As seen in phase contrast, calcein staining of live cells decreased markedly and proportionally to the dose of FTLD-TDP-A-extracted aggregates, whereas control and FTLD-TDP-C SarkoSpin pellet inoculations had no effect. This specific neurotoxic effect of FTLD-TDP-A aggregates was measured both by the decrease of cell body number (Fig. 6g) and neurite length (Fig. 6h) in a dose-dependent manner.

Collectively, our data indicate that pathological TDP-43 adopts stable configurations with specific biophysical properties that allow its physical separation from its physiological counterpart. Notably, the biochemical properties of pathological TDP-43 and a subset of insoluble proteins can discriminate between specific neuropathological subtypes, indicating that they may underlie specific disease characteristics. Most important, we show that pTDP-43 aggregates extracted by our new purification method confer cytotoxicity or neurotoxicity accompanied by induced aggregation of endogenous TDP-43. Notably, the most toxic aggregates are those found in the brains of FTLD-TDP-A subjects, who show significantly shorter disease duration (Supplementary Fig. 1c), suggesting a link between the properties of TDP-43 aggregates and clinical presentation.

Discussion

TDP-43 pathology characterizes most instances of ALS and FTLD and its spatiotemporal manifestation coincides with neurodegeneration, supporting its central pathogenic role in these diseases[41]. Despite this unifying TDP-43 pathology, ALS and FTLD subjects display large heterogeneity in terms of clinical presentation, progression and neuropathological findings, a phenomenon that remains mechanistically unexplained. Recent discoveries indicate that several protein aggregation diseases follow a prion-like paradigm[42] through amplification of pathological conformers. These findings provide a plausible explanation of the origin of disease heterogeneity. Indeed, differential quaternary structures of the prion protein are responsible for different subtypes of infectious prion diseases and are associated with distinct neuropathological profiles and clinical presentations[38]. The notion of prion strains was recently expanded to other protein aggregation diseases, with compelling data for tau[43], α-synuclein[44] and amyloid-β[45].

We show that human subject–derived TDP-43 adopts stable protein assemblies with specific biophysical properties. We exploited these features to develop SarkoSpin, a method for the isolation of TDP-43 aggregates and their separation from physiological complexes. All pathological features described thus far for TDP-43 (namely insolubility, hyperphosphorylation, polyubiquitination and proteolytic cleavage) were concentrated in the SarkoSpin purified fraction. However, we cannot formally exclude the possibility that soluble pathogenic TDP-43 assemblies with yet undescribed pathological features escape our method and remain in the supernatant. Nevertheless, we think SarkoSpin will become a valuable tool for any application requiring authentic human disease-associated TDP-43 aggregates. An unbiased proteomic analysis of isolated pathological assemblies revealed that TDP-43 was the most significantly enriched protein and the only one found to be insoluble in all disease cases, indicating that we isolated the pTDP-43 core of pathological assemblies. By comparing other proteins that become insoluble in ALS and FTLD human brains, we found specific subclasses of proteins characterizing each disease subtype. These proteins did not colocalize with pTDP-43 in subject brains and sometimes even occurred in different cell types, such as FBXO2 in astrocytes, suggesting that they probably represent a molecular signature originating from the divergent pathogenic mechanisms characterizing these disease subtypes.

By combining SarkoSpin with a number of biochemical, molecular and imaging methodologies, we provide evidence that TDP-43 extracted from different disease subtypes exhibits distinct biochemical and morphological features. In particular, the intrinsic density of the isolated particles is notably consistent within each disease subtype and is a distinctive feature of pathological TDP-43 in different FTLD types. Our results indicate that FTLD-TDP-C, an exclusively sporadic type of dementia with significantly longer disease duration than other types[21], is associated with very dense TDP-43 aggregates with lower levels of polyubiquitination and a highly protease-resistant C-terminal core, as compared to TDP-43 assemblies extracted from FTLD-TDP-A or ALS. Although no long fibrillary structures were detected within TDP-43 aggregates of either disease subtype, short proteinaceous filaments were present in both, albeit with different accessibility to specific antibodies, indicating alternate aggregate packaging. To our surprise, the neuropathological type predicted the features of TDP-43 aggregates better than genetic mutations did, indicating that the same genetic trigger may give rise to variable pathological assemblies, which are perhaps determined by other, unknown factors.

Fig. 6 | Differential cyto- and neurotoxicity of FTLD-TDP type A and type C pathological assemblies. a, Schematic representation of SarkoSpin inoculations on arrested HEK293 cells expressing TDP-43-HA. **b**, Viability ratio of cells with doxycycline-induced expression of TDP-43-HA (+DOX) or without it (–DOX). Each point represents the viability ratio of cells inoculated with the SarkoSpin pellet of a single subject; $n=6$, $n=9$ and $n=7$ biologically independent human brain samples for control, FTLD-TDP-A and FTLD-TDP-C groups, respectively, Bars show mean ± s.d., after normal distribution and equal variance verifications (Shapiro–Wilk and *F*-test), two-sided unpaired *t* test gave the indicated *P* value. **c**, Immunoblots of SarkoSpin supernatants and pellets from TDP-43-HA-expressing cells inoculated with SarkoSpin pellet pools extracted from control ($n=3$), FTLD-TDP-A ($n=3$) or FTLD-TDP-C ($n=3$) subjects. Full-size blots are in Supplementary Fig. 18h. **d**, Schematic of neurite outgrowth and toxicity assay on mouse primary cortical neuronal cultures upon inoculations of SarkoSpin pellets from different disease subtypes. **e**–**h**, $n=3$ biologically independent human brain samples for control (black), FTLD-TDP-A (green) and FTLD-TDP-C (blue), used for cell inoculations in three independent experiments. **e**, Representative fluorescence calcein (green, upper rows) images and corresponding neurite and cell body segments (blue and yellow respectively, lower rows) for control (top), FTLD-TDP-A (middle) and FTLD-TDP-C (bottom) SarkoSpin pellet inoculations at indicated total protein amounts at 10 DIV endpoint. **f**, Dynamics of neurite outgrowth revealed by quantification of the phase contrast images of inoculated neurons at 0.3 µg total protein dose per well (error bars show mean and s.d.). Two-way ANOVA of all groups with Tukey's corrections for each time point revealed that FTLD-TDP-A was significantly different from control from day 5 on (*P* values for days 5–10, respectively: $P=0.014$; 1.3×10^{-3}; 1.5×10^{-4}; 3.75×10^{-7}; 1.90×10^{-12}; 8.07×10^{-13}). **g**,**h**, Quantification of the endpoint calcein fluorescence images using a cell body (**g**) or neurite length (**h**) segmentation algorithm for different doses of SarkoSpin extracts (error bars show mean and s.d.). Two-way ANOVA followed by Tukey's multiple-comparison tests showed that all FTLD-TDP-A, but not FTLD-TDP-C, values are significantly different from control (*P* values for 0–1 µg doses: **g**, 0 µg, $P=0.14$; 0.03 µg, $P=2\times10^{-3}$; 0.1 µg, $P=9.5\times10^{-7}$; 0.3 µg, $P=1.1\times10^{-8}$; 1 µg, $P=6.2\times10^{-9}$; **h**, 0 µg, $P=0.87$; 0.03 µg, $P=10^{-4}$; 0.1 µg, $P=1.7\times10^{-9}$; 0.3 µg, $P=1.2\times10^{-11}$; 1 µg, $P=4.3\times10^{-13}$). For **c**,**e**, experiments were independently repeated two and three times, respectively, with similar results.

Most critically, the biochemical and morphological differences between FTLD-TDP-A and FTLD-TDP-C pTDP-43 assemblies were associated with differential seeding and neurotoxic potential. Indeed, FTLD-TDP-A aggregates extracted from subjects with fast-progressing disease caused toxicity and induced endogenous TDP-43 aggregation in cellular models, whereas FTLD-TDP-C aggregates from slow-progressing disease seemed inert under the same conditions and equivalent pTDP-43 doses. In the future, by following the paradigm now established for several other protein aggregates[43–45], we could find out whether these subject-derived TDP-43 pathological conformations can propagate in vivo, reproducing their distinctive features and disease phenotypes in animal models. Additional work is necessary to establish a direct link between TDP-43 pathological characteristics and disease subtypes. However, our

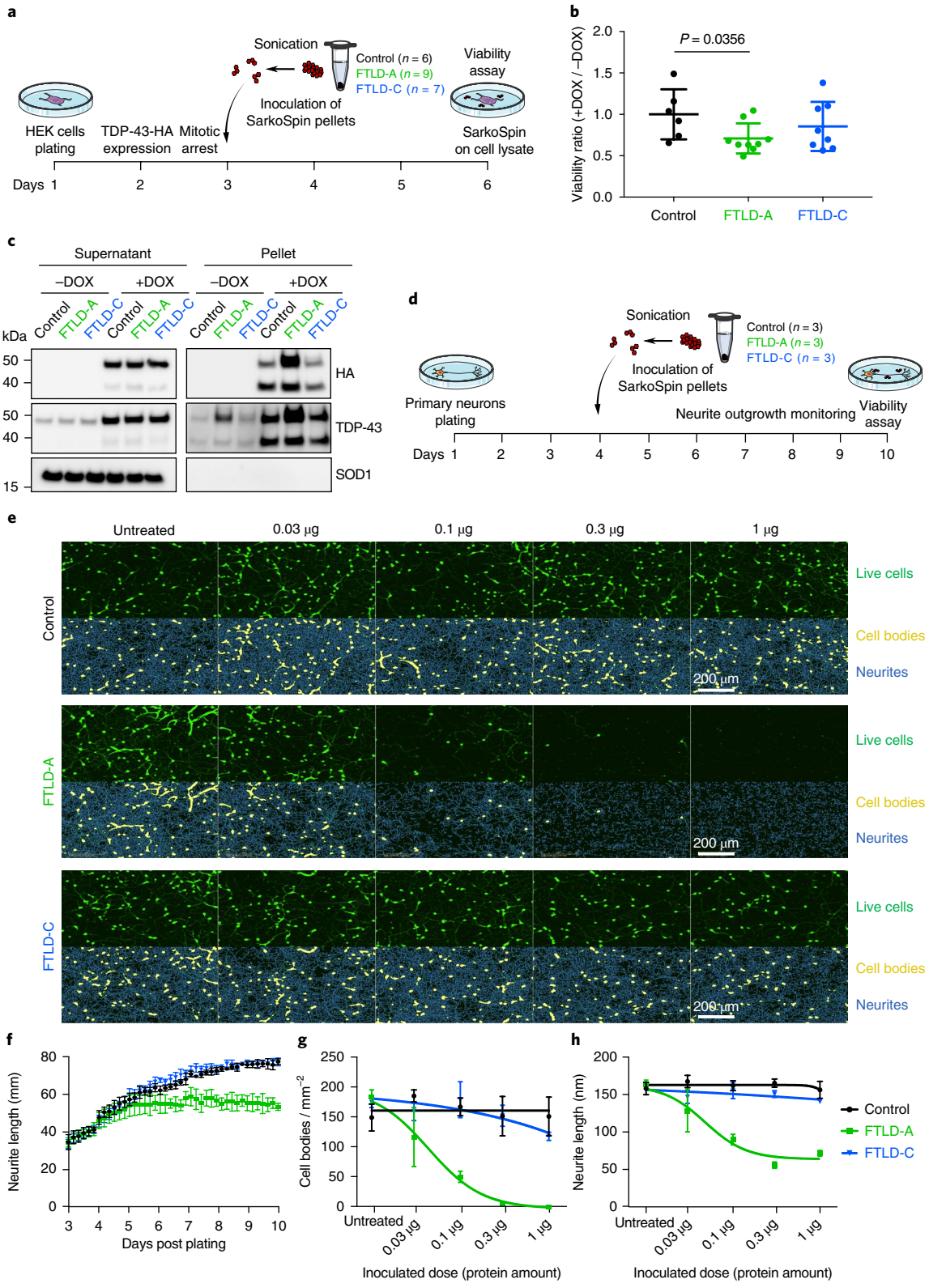

work is compatible with the idea that disease heterogeneity could originate from alternate pathological TDP-43 conformations, as has been observed in the case of prion strains, and opens new avenues for creating cellular and animal models.

Online content

Any methods, additional references, Nature Research reporting summaries, source data, statements of data availability and associated accession codes are available at https://doi.org/10.1038/s41593-018-0294-y.

Received: 10 September 2018; Accepted: 14 November 2018;
Published online: 17 December 2018

References

1. Ling, S. C., Polymenidou, M. & Cleveland, D. W. Converging mechanisms in ALS and FTD: disrupted RNA and protein homeostasis. *Neuron* **79**, 416–438 (2013).
2. Neumann, M. et al. Ubiquitinated TDP-43 in frontotemporal lobar degeneration and amyotrophic lateral sclerosis. *Science* **314**, 130–133 (2006).
3. Arai, T. et al. TDP-43 is a component of ubiquitin-positive tau-negative inclusions in frontotemporal lobar degeneration and amyotrophic lateral sclerosis. *Biochem. Biophys. Res. Commun.* **351**, 602–611 (2006).
4. Buratti, E. et al. Nuclear factor TDP-43 and SR proteins promote in vitro and in vivo CFTR exon 9 skipping. *EMBO J.* **20**, 1774–1784 (2001).
5. Polymenidou, M. et al. Long pre-mRNA depletion and RNA missplicing contribute to neuronal vulnerability from loss of TDP-43. *Nat. Neurosci.* **14**, 459–468 (2011).
6. Tollervey, J. R. et al. Characterizing the RNA targets and position-dependent splicing regulation by TDP-43. *Nat. Neurosci.* **14**, 452–458 (2011).
7. Afroz, T. et al. Functional and dynamic polymerization of the ALS-linked protein TDP-43 antagonizes its pathologic aggregation. *Nat. Commun.* **8**, 45 (2017).
8. Jiang, L. L. et al. The N-terminal dimerization is required for TDP-43 splicing activity. *Sci. Rep.* **7**, 6196 (2017).
9. Gu, J. et al. Transactive response DNA-binding protein 43 (TDP-43) regulates alternative splicing of tau exon 10: Implications for the pathogenesis of tauopathies. *J. Biol. Chem.* **292**, 10600–10612 (2017).
10. Ederle, H. & Dormann, D. TDP-43 and FUS en route from the nucleus to the cytoplasm. *FEBS Lett.* **591**, 1489–1507 (2017).
11. Dewey, C. M. et al. TDP-43 is directed to stress granules by sorbitol, a novel physiological osmotic and oxidative stressor. *Mol. Cell. Biol.* **31**, 1098–1108 (2011).
12. Alami, N. H. et al. Axonal transport of TDP-43 mRNA granules is impaired by ALS-causing mutations. *Neuron* **81**, 536–543 (2014).
13. Gopal, P. P., Nirschl, J. J., Klinman, E. & Holzbaur, E. L. Amyotrophic lateral sclerosis-linked mutations increase the viscosity of liquid-like TDP-43 RNP granules in neurons. *Proc. Natl Acad. Sci. USA* **114**, E2466–E2475 (2017).
14. Kato, M. et al. Cell-free formation of RNA granules: low complexity sequence domains form dynamic fibers within hydrogels. *Cell* **149**, 753–767 (2012).
15. Molliex, A. et al. Phase separation by low complexity domains promotes stress granule assembly and drives pathological fibrillization. *Cell* **163**, 123–133 (2015).
16. Igaz, L. M. et al. Enrichment of C-terminal fragments in TAR DNA-binding protein-43 cytoplasmic inclusions in brain but not in spinal cord of frontotemporal lobar degeneration and amyotrophic lateral sclerosis. *Am. J. Pathol.* **173**, 182–194 (2008).
17. Neumann, M. et al. Phosphorylation of S409/410 of TDP-43 is a consistent feature in all sporadic and familial forms of TDP-43 proteinopathies. *Acta Neuropathol.* **117**, 137–149 (2009).
18. Lashley, T., Rohrer, J. D., Mead, S. & Revesz, T. Review: an update on clinical, genetic and pathological aspects of frontotemporal lobar degenerations. *Neuropathol. Appl. Neurobiol.* **41**, 858–881 (2015).
19. Neary, D. et al. Frontotemporal lobar degeneration: a consensus on clinical diagnostic criteria. *Neurology* **51**, 1546–1554 (1998).
20. Mackenzie, I. R. & Neumann, M. Reappraisal of TDP-43 pathology in FTLD-U subtypes. *Acta Neuropathol.* **134**, 79–96 (2017).
21. Lee, E. B. et al. Expansion of the classification of FTLD-TDP: distinct pathology associated with rapidly progressive frontotemporal degeneration. *Acta Neuropathol.* **134**, 65–78 (2017).
22. Nonaka, T. et al. Prion-like properties of pathological TDP-43 aggregates from diseased brains. *Cell Rep.* **4**, 124–134 (2013).
23. Tsuji, H. et al. Molecular analysis and biochemical classification of TDP-43 proteinopathy. *Brain* **135**, 3380–3391 (2012).
24. Laferrière, F. et al. Quaternary structure of pathological prion protein as a determining factor of strain-specific prion replication dynamics. *PLoS Pathog.* **9**, e1003702 (2013).
25. Polymenidou, M. et al. Coexistence of multiple PrPSc types in individuals with Creutzfeldt-Jakob disease. *Lancet Neurol.* **4**, 805–814 (2005).
26. Carra, S. et al. Alteration of protein folding and degradation in motor neuron diseases: Implications and protective functions of small heat shock proteins. *Prog. Neurobiol.* **97**, 83–100 (2012).
27. Neumann, M. et al. Absence of heterogeneous nuclear ribonucleoproteins and survival motor neuron protein in TDP-43 positive inclusions in frontotemporal lobar degeneration. *Acta Neuropathol.* **113**, 543–548 (2007).
28. Kametani, F. et al. Mass spectrometric analysis of accumulated TDP-43 in amyotrophic lateral sclerosis brains. *Sci. Rep.* **6**, 23281 (2016).
29. Ingre, C. et al. A novel phosphorylation site mutation in profilin 1 revealed in a large screen of US, Nordic, and German amyotrophic lateral sclerosis/frontotemporal dementia cohorts. *Neurobiol. Aging* **34**, 1708.e1–1708.e6 (2013).
30. Wu, C. H. et al. Mutations in the profilin 1 gene cause familial amyotrophic lateral sclerosis. *Nature* **488**, 499–503 (2012).
31. Zhou, J. et al. Spinal muscular atrophy associated with progressive myoclonic epilepsy is caused by mutations in ASAH1. *Am. J. Hum. Genet.* **91**, 5–14 (2012).
32. Xu, G., Stevens, S. M. Jr., Moore, B. D., McClung, S. & Borchelt, D. R. Cytosolic proteins lose solubility as amyloid deposits in a transgenic mouse model of Alzheimer-type amyloidosis. *Hum. Mol. Genet.* **22**, 2765–2774 (2013).
33. McGurk, L. et al. Poly-A binding protein-1 localization to a subset of TDP-43 inclusions in amyotrophic lateral sclerosis occurs more frequently in patients harboring an expansion in C9orf72. *J. Neuropathol. Exp. Neurol.* **73**, 837–845 (2014).
34. Kerman, A. et al. Amyotrophic lateral sclerosis is a non-amyloid disease in which extensive misfolding of SOD1 is unique to the familial form. *Acta Neuropathol.* **119**, 335–344 (2010).
35. Robinson, J. L. et al. TDP-43 skeins show properties of amyloid in a subset of ALS cases. *Acta Neuropathol.* **125**, 121–131 (2013).
36. Lin, W. L. & Dickson, D. W. Ultrastructural localization of TDP-43 in filamentous neuronal inclusions in various neurodegenerative diseases. *Acta Neuropathol.* **116**, 205–213 (2008).
37. Guenther, E. L. et al. Atomic structures of TDP-43 LCD segments and insights into reversible or pathogenic aggregation. *Nat. Struct. Mol. Biol.* **25**, 463–471 (2018).
38. Aguzzi, A., Heikenwalder, M. & Polymenidou, M. Insights into prion strains and neurotoxicity. *Nat. Rev. Mol. Cell Biol.* **8**, 552–561 (2007).
39. Yagi, H. et al. Zonisamide enhances neurite elongation of primary motor neurons and facilitates peripheral nerve regeneration in vitro and in a mouse model. *PLoS One* **10**, e0142786 (2015).
40. Danzer, K. M., Krebs, S. K., Wolff, M., Birk, G. & Hengerer, B. Seeding induced by alpha-synuclein oligomers provides evidence for spreading of alpha-synuclein pathology. *J. Neurochem.* **111**, 192–203 (2009).
41. Polymenidou, M. & Cleveland, D. W. Biological spectrum of amyotrophic lateral sclerosis prions. *Cold Spring Harb. Perspect. Med.* **7**, a024133 (2017).
42. Polymenidou, M. & Cleveland, D. W. The seeds of neurodegeneration: prion-like spreading in ALS. *Cell* **147**, 498–508 (2011).
43. Sanders, D. W. et al. Distinct tau prion strains propagate in cells and mice and define different tauopathies. *Neuron* **82**, 1271–1288 (2014).
44. Peelaerts, W. et al. α-Synuclein strains cause distinct synucleinopathies after local and systemic administration. *Nature* **522**, 340–344 (2015).
45. Meyer-Luehmann, M. et al. Exogenous induction of cerebral beta-amyloidogenesis is governed by agent and host. *Science* **313**, 1781–1784 (2006).

Acknowledgements

We are grateful to all the subjects and their families for donating tissues for scientific research; this work would not have been possible without their generosity and foresightedness. We thank S. Saberi and M.J. Rodriguez from UCSD for preparing and shipping autopsy material from San Diego to Zurich; A. Käch and the Center for Microscopy and Image Analysis of the University of Zurich for help and technical support in all electron microscopy experiments; H. Leske, K. Frontzek, E. Rushing and A. Aguzzi (Institute of Neuropathology, University Hospital of Zurich) for helpful advice and discussions; J. Luedke and J. Weber for technical help; and S. Sahadevan M.K. and A. Zbinden for critical input on the manuscript. We thank M. Gstaiger (Institute of Molecular Systems Biology, ETH Zurich, Switzerland) for sharing the Flp-In T-REx HEK293 cell line and the pOG44 plasmid. This work was supported by a Swiss National Science Foundation Professorship (PP00P3_144862) and a Human Frontier Science Program Career Development Award (CDA-00058/2012) to M.P. and a UCL/ZNZ Neuroscience Collaboration Grant to M.P and A.M.I funded through UCL's Wellcome Trust Institutional Strategic Support Fund Investing in Excellent Researchers (105604/Z/14/Z). F.L. and M.H.P. are both recipients of the Milton-Safenowitz fellowship from the ALS Association (15-IIP-208 and 16-PDF-247, respectively). F.L. received a

Postdoc Award and Z.M. a Candoc Award (Forschungskredit) from the University of Zurich. T.L. is funded by an Alzheimer's Research UK senior fellowship. Y.T.A. was supported by the Leonard Wolfson Centre for experimental neurology. A.I. is the recipient of a European Research Council consolidator grant (648716-C9ND). The Queen Square Brain Bank is supported by the Reta Lila Weston Institute for Neurological Studies and the Progressive Supranuclear Palsy (Europe) Association.

Author contributions

F.L. developed and performed the biochemical experiments with the help of Z.M. and M.P. conceived and directed the study. M.P.-B. generated and characterized the stable cell line with inducible TDP-43-HA and performed cell toxicity experiments. M.H.-P., L.G., E-M.H., and T.A. helped with performing gradients and developing the SarkoSpin method. P.B. and P.P. performed mass spectrometry, which was bioinformatically analyzed by U.W. G.B. performed electron microscopy experiments. A.A.-A., A.L. and H.S. gave critical input on the structural analysis of extracted aggregates by electron microscopy and performed preliminary cryo-electron microscopy and correlative light-electron microscopy experiments. Autopsy material and associated clinical and neuropathological information was provided by J.R., T.L. and A.I., while S.C.F. carried out the pTDP-43 immunohistochemistry and immunofluorescence and Y.T.A. sampled the cases from the Queen Square Brain Bank. F.D.G., F.I. and E.B. performed and analyzed inoculations on primary neurons. F.L., Z.M. and M.P wrote the manuscript. All authors read, edited and approved the final manuscript.

Competing interests

The authors declare no competing financial interests.

Additional information

Supplementary information is available for this paper at https://doi.org/10.1038/s41593-018-0294-y.

Reprints and permissions information is available at www.nature.com/reprints.

Correspondence and requests for materials should be addressed to M.P.

Publisher's note: Springer Nature remains neutral with regard to jurisdictional claims in published maps and institutional affiliations.

Methods

Cases. Brains were donated to the Queen Square Brain Bank for Neurological disorders, Department of Movement Disorders, UCL Institute of Neurology, or the Department of Neurology, University of California San Diego, or the Netherlands Brain Bank, Netherlands Institute for Neuroscience (open access: http://www.brainbank.nl). All subject material was collected from donors for or from whom a written informed consent for a brain autopsy and the use of the material and clinical information for research purposes has been obtained by the respective institution. No statistical methods were used to predetermine sample sizes. Instead, we used the maximum number of samples that were available to us.

Antibodies. All antibodies we used are listed with suppliers, clone or catalog numbers and dilutions used in Supplementary Table 2. Each antibody was validated for the species (human or mouse) and application (WB, western blot; DB, dot blot; IF, immunofluorescence; IHC, immunohistochemistry) by the corresponding manufacturer.

Immunohistochemistry. Fresh tissue from frontal cortex of FTLD-TDP-A cases, either sporadic or with *C9orf72* mutation, as well as a FTLD-TDP-C cases was fixed with phosphate-buffered 3.65% formaldehyde, embedded in paraffin, cut into 6-µm serial sections and mounted on glass slides. Sections were deparaffinized and rehydrated using a gradient of alcohol. Antigen retrieval was done by boiling the sections in 10 mM citrate buffer, pH 6.0, in a microwave oven. Immunohistochemistry was performed using the avidin–biotin complex detection system (Vector Laboratories) and 3,3-diaminobenzidine. Endogenous peroxidases were first quenched with 5% H_2O_2 in methanol for 30 min, and then sections were blocked in 0.1 mol l^{-1} Tris with 2% FBS for 5 min. Primary antibodies were incubated for 2 h at room temperature. After washing, sections were sequentially incubated with biotinylated secondary antibodies for 1 h and avidin–biotin complex for 1 h. Bound antibody complexes were visualized by incubation of sections in a solution containing 100 mM Tris, pH 7.6, 0.1% Triton X-100, 1.4 mM diaminobenzidine, 10 mM imidazole and 8.8 mM H_2O_2. Sections were then lightly counterstained with hematoxylin, dehydrated and coverslipped. Digital images were obtained using Life Technologies EVOS FL Auto imaging system (Life Technologies).

All antibodies used for immunofluorescence and western blots are listed in Supplementary Table 2 with the respective catalog numbers and working dilutions indicated for each assay.

Homogenization of brain tissue. Frozen tissue from motor or frontal cortex of all groups of subjects was homogenized at 20% (w/v) in homogenization-solubilization (HS) buffer without detergent: 10 mM Tris, pH 7.5, 150 mM NaCl, 0.1 mM EDTA, 1 mM dithiothreitol, complete EDTA-free protease inhibitors (Roche) and PhosSTOP phosphatase inhibitors (Roche). Samples were subjected to three rounds of 30 s homogenization in tubes containing a mixture of ceramic beads of 1.4 and 2.8 mm of diameter on a Minilys device (Bertin) at full speed with cooling on ice between each round. Samples were aliquoted, snap frozen in liquid nitrogen and kept at −80 °C before use.

SarkoSpin on subject tissues. All SarkoSpin steps were done in 1.5 ml Protein Low Binding tubes (Eppendorf). Brain homogenate aliquots of 150 µl were thawed on ice and equalized for protein concentration in a final volume of 200 µl using HS buffer. Samples were then diluted 1:1 in HS buffer with 4% (w/v) *N*-lauroyl-sarcosine (sarkosyl, Sigma), 2 U μl^{-1} Benzonase (Novagen) and 4 mM $MgCl_2$, reaching a final volume of 400 µl with final concentrations of 2% sarkosyl, 1 U μl^{-1} Benzonase and 2 mM $MgCl_2$. SarkoSpin solubilization was then performed by incubating the samples at 37 °C under constant shaking at 600 r.p.m. (Thermomixer, Eppendorf) for 45 min. Solubilized brain homogenates (400 µl) were then further diluted by adding 200 µl of ice-cold HS buffer containing 0.5% (w/v) sarkosyl before centrifugation at 21,200*g* on a benchtop centrifuge (Eppendorf) for 30 min at room temperature. Alternatively, for electron microscopy sample preparation, to keep lipids from precipitating along with protein aggregates, solubilized material was overlaid on 400 µl sucrose cushion (40% (w/v) sucrose (Sigma) in HS buffer containing 0.5% (w/v) sarkosyl) and centrifuged at 21,200*g* for 1 h at room temperature. For analysis of proteolytic profiles, after the initial 15 min of SarkoSpin solubilization, the respective protease was added for the remaining 30 min of incubation at the following final concentrations: 100 µg ml^{-1} proteinase K, 10 µg ml^{-1} chymotrypsin or 100 µg ml^{-1} trypsin (from stock solutions of 2 mg ml^{-1}, 0.2 mg ml^{-1} or 2 mg ml^{-1}, respectively). Supernatants (~600 µl) were collected in a new tube and pellets were resuspended in desired volume of HS buffer containing 0.5% (w/v) sarkosyl for further analysis, including dot blot, SDS–PAGE and immunoblot or native PAGE. Whenever specified, the fractions were passed through low-protein-binding 0.22 µm filters (Millex-GV) to remove large nonsolubilized particles.

SarkoSpin on cells. Transfected NSC-34 cells in 10 cm dishes (see below) were lysed in 400 µl of ice-cold 1× HS buffer with 0.5% sarkosyl, 2 mM $MgCl_2$ and ~100 U Benzonase, and 60 µl of the lysate was put aside for protein concentration measurements and immunoblots. For SarkoSpin of inoculated HEK 293 cells, cells plated in a 6-well plate were lysed in 170 µl of ice-cold 1× HS buffer with 0.5% sarkosyl, 2 mM $MgCl_2$ and ~25 U Benzonase per well. For sample solubilization, 52 µl 1× HS and 178 µl 2X HS with 4% sarkosyl were added to aliquots of 170 µl of lysate for a final concentration of 2% sarkosyl in 400 µl of sample. After a 30-min incubation on ice with vortexing every 10 min, the samples were diluted by adding 200 µl of ice-cold HS buffer and centrifuged as described before for SarkoSpin on brain homogenates. Supernatants were collected in a new tube and pellets were resuspended in 1× HS buffer with 0.5% sarkosyl for immunoblot samples or in PBS for inoculation experiments in HEK 293 cells. SarkoSpin fractions from cell line experiments were processed for immunoblots as described before for brain homogenates.

Mass spectrometry. After cleanup with C18 cartridges, the peptide samples were measured on a TripleTOF 5600 instrument (AB Sciex) equipped with a nanoelectrospray ion source and an Eksigent 1D-plus liquid chromatography system (Eksigent) or a Q Exactive Plus instrument (Thermo Fisher) equipped with an EASY-nLC 1000 (Thermo Fisher). For the TripleTOF measurements, peptides were loaded onto a 20-cm-long, 75-µm internal diameter (i.d.) PicoFrit Column (New Objective) packed in-house with Magic C18 AQ 3-µm beads (Michrom Bioresources) and separated with a linear gradient of 5–35% acetonitrile in 90 min at a flow rate of 300 nl min^{-1}. Survey scans were acquired in 300 ms and up to 20 product ion scans were collected in 75 ms when exceeding a threshold of 150 counts per second with a charge state from 2^+ to 5^+. For the Q Exactive Plus measurements, peptides were loaded on a 40-cm-long, 75-µm i.d. column packed in-house with ReproSil-Pur C18-AQ resin (1.9 µm, Dr. Maisch). Peptides were eluted for 50 min using a segmented linear gradient of 5–40% acetonitrile at a flow rate of 300 nl min^{-1}. Survey full-scan mass spectra were acquired with mass range 350–1,500 *m/z*, at a resolution of 70,000 at 200 *m/z*, and the 20 most intense ions above an intensity of 3.6×10^4 were sequentially isolated, fragmented (HCD at 25 NCE) and measured at a resolution of 17,500 at 200 *m/z*. Peptides with a charge of +1 or with unassigned charge state were excluded from fragmentation for MS2, and a dynamic exclusion of 30 s was applied. Ions were accumulated to target values of 3×10^6 for MS1 and of 1×10^5 for MS2.

MGF peak lists generated from the acquired spectra by ProteinPilot from the TripleTOF runs and RAW files from the Q Exactive Plus runs were searched for in a human Uniprot protein database (68978 sequence) by Sequest HT in Proteome Discoverer 1.4 (Thermo Scientific) with enzymatic specificity of trypsin, precursor mass tolerance of 20 p.p.m. and fragment tolerance of 0.1 Da and 0.02 Da for TripleTOF and Q Exactive Plus, respectively. Methionine oxidation and carbamidomethylation of cysteines were set as variable and static modifications, respectively. Percolator was used to filter the results to a 1% peptide false discovery rate. Spectral counting was used for quantifying protein differences between samples.

Statistical analysis of mass spectrometry data. Unless stated otherwise the higher-level data analysis was carried out using R/Bioconductor (R Core Team, 2017). The count values for each sample were normalized by dividing the values by the respective trimmed mean (removing the 5% highest and lowest values). As the samples were run in two separate batches, the ComBat method[46] was applied to correct for the batch effect. To identify proteins that were most consistently enriched in subject samples, we established an idealized vector correlation method: a vector of the same number of zeroes as control samples and the same number of ones as subject samples was created. For each protein, we measured the correlation of this idealized vector with the vector of normalized and batch-corrected protein abundance values of control and subject samples. We then selected the 50 best-correlated proteins and established a heatmap of the $\log_2$ abundance values. For the heatmap, we applied a median per protein normalization by dividing the values of each protein by the respective median values of the control samples.

Validation of mass spectrometry hits by immunofluorescence. Formalin-fixed paraffin-embedded tissue was sectioned at 7 µm. Sections were deparaffinized in xylene and rehydrated using a gradient of alcohol. Endogenous peroxidases were first quenched with 0.3% H_2O_2 in methanol for 10 min. Antigen retrieval was undertaken in a pressure cooker for 10 min at maximum pressure in 10 mM citrate buffer, pH 6.0, and sections were blocked in 10% nonfat milk for 30 min. Sections were incubated with phosphorylation-specific rabbit polyclonal antibody to pTDP (pSer409, 1:20,000, Cosmobio). After washing, sections were sequentially incubated with biotinylated swine anti-rabbit secondary antibody for 30 min and avidin–biotin complex for 30 min. pTDP-43 was visualized using TSA Rhodamine amplification (Perkin-Elmer) at 1:500 for 30 min. Sections were then incubated with antibodies to TLXN1, FBXO2 or ASAH1 followed by incubation with AlexaFluor 468-coupled secondary antibodies at 1:1,000 for 1 h at room temperature. Sections were viewed and imaged with a Leica TCS4D using a three-channel scan head fluorescent microscope and images were deconvoluted using Leica software.

Velocity sedimentation and density floatation gradients. Brain homogenates were thawed on ice and solubilized as described previously (SarkoSpin). For velocity sedimentations, a volume of 200 µl was loaded on top of a 4-ml continuous 10–25% iodixanol gradient (Optiprep, Sigma) in HS buffer with 0.5% (w/v) sarkosyl linearized directly in 4.2-ml ultracentrifuge tubes (Seton) with a Gradient

Master (Biocomp). For density floatation gradients, 220 µl of HS buffer with 40% iodixanol and 0.5% (w/v) sarkosyl was loaded within a 4-ml 10–60% discontinuous iodixanol gradient in HS buffer with 0.5% (w/v) sarkosyl. The gradients were centrifuged at 310,000*g* for 45 min (velocity) or at 125,000*g* for 17 h (density) in a swinging-bucket SW-60 Ti rotor using an Optima XPN-100 ultracentrifuge (Beckman Coulter). Gradients were then segregated into 16 equal fractions from the top using a piston fractionator (Biocomp) and a fraction collector (Gilson). Fractions were aliquoted for further analysis of their content by dot blot, immunoblot on SDS–PAGE or native PAGE. Gradient linearity was verified by refractometry.

Analysis of protein content of SarkoSpin, velocity and density fractions. Aliquots of the collected fractions were mixed with SDS–PAGE loading buffer with reducing agent (Life Technologies) and denatured at 95 °C for 5 min before migration on Bolt 12% Bis-Tris gels (Life Technologies). For visualizing total proteins, gels were stained with silver nitrate. For immunoblots, gels were electrotransferred onto nitrocellulose membranes with iBlot 2 (Life Technologies). For dot blotting, native fractions were spotted onto nitrocellulose 0.2-µm membranes using a dot blot vacuum device (Whatman). Nitrocellulose membranes were blocked with 5% (w/v) skimmed powder milk (or 5% (w/v) BSA for antibody to pSer409 or pSer410) in PBS-Tween and probed with primary and secondary antibodies (Supplementary Table 2). Immunoreactivity was visualized by chemiluminescence (GE Healthcare). The amount of the respective protein in each fraction was determined by Image Studio Lite software after acquisition of chemiluminescent signals with a Fuji LAS 4000 digital imager (GE Healthcare). Profiles obtained by immunoblot were normalized and plotted with s.d., with all respective Student's tests and analysis of variance (ANOVA) using Prism software. Fractions were also subjected to native-PAGE immunoblotting, for which aliquots were mixed with native sample buffer and G250 additive (Life Technologies) and resolved using 3–12% Bis-Tris Native-PAGE gels (Life Technologies) and NativeMark protein ladder (Life Technologies). Gels were incubated with 2× transfer buffer and electrotransferred with iBlot 2 on polyvinylidene difluoride membranes. After fixation with 8% acetic acid, air-drying and reactivation with methanol, membranes were immunoblotted and probed as described above.

Transmission electron microscopy. SarkoSpin pellets from different disease types and control subjects were resuspended in water and passed through low-protein-binding 0.22-µm syringe filters. The resulting filtrates were fixed with glutaraldehyde water solution (EMS, 16220; final concentration of 0.05%) and subjected to immuno-gold labeling. A 300-mesh copper grid (Plano, G2300C), formvar coated and glow discharged, was put on a 3-µl drop of fixed sample for 3 min. The grid was then washed three times for 20 s in aldehyde blocking solution with 0.15% glycine (Sigma, G7126) in PBS and three times for 20 s in PBS, followed by 5 min incubation in blocking solution (PBG): PBS with 0.2% gelatin (Sigma, G6650) and 0.5% BSA (Applichem, A6588). The grid was probed with TDP-43 60019-2-Ig (mouse 1:50 in PBG solution, Proteintech) for 20 min (the negative control without primary antibody was incubated instead in PBG solution). The grid was washed in PBG solution three times for 20 s, and incubated for another 5 min in PBG, before probing with secondary anti-mouse antibody coupled with 12 nm gold beads (1:20 in PBG solution, Jackson ImmunoResearch, 115-205-146) for 20 min. The grid was washed four times for 20 s in PBG and twice for 20 s in PBS, followed by a second fixation step for 30 s in 0.1% glutaraldehyde in PBS, and then washed in water four times for 20 s. The grid was then counterstained with 1% uranyl acetate (Fluka, 73943) in water for 1 min. Excess solution was sucked off using filter paper and the grid was air dried. Alternatively, to avoid drying artifacts, the counterstaining solution included 1.8% methylcellulose (Sigma) in water and 0.3% uranyl acetate in water (incubation for 3 min staining procedure on ice). Last, the grid was picked up with a loop, excess solution was sucked off with filter paper, the grid was air dried, and the specimen was imaged with a CM100 transmission electron microscope (Thermo Fisher Scientific) at an acceleration voltage of 80 kV using a Gatan Orius 1000 digital camera (Gatan).

Plasmid generation. A multiply tagged TDP-43-encoding pcDNA5 plasmid[47] was modified to obtain a sequence coding for a single C-terminally HA-tagged TDP-43. The N-terminal GFP, His_6 and myc tags and the residual C-terminal amino acids between the HA tag and the stop codon were deleted in two subsequent reactions using the Q5 Site-Directed Mutagenesis kit (New England Biolabs, E0554S) according to the manufacturer's instructions, with the following primers: 5′-TCT GAA TAT ATT CGG GTA ACC GAA GAT GAG AAC GAT GAG-3′, 5′- CAT CCG CGG GGC AGG GGT-3′ (tags, annealing temperature Ta = 72 °C), 5′-TAA ACC CGC TGA TCA GCC-3′, 5′-AGC ATA ATC AGG GAC ATC ATA AG-3′ (residual amino acids, Ta = 63 °C).

Cell culture, stable cell line generation and transient transfection. HEK293 Flp-In T-REx cells (Invitrogen, R78007) were cultured in DMEM (Sigma, D5671) supplemented with 10% FBS (Gibco, 10270-106), 1× penicillin-streptomycin (Gibco, 15140-122), 1× GlutaMAX (Gibco, 35050061), 15 µg ml^{-1} blasticidin S (Gibco, R21001; Invivogen, ant-bl-10p) and 100 µg ml^{-1} zeocin (Gibco, R25001). To generate a stable cell line expressing HA-tagged TDP-43, 3×10^5 cells were plated per well in a 6-well plate and transfected after 48 h with 125 ng of pcDNA5-TDP43-HA plasmid and 1,125 ng of pOG44 plasmid with 6.25 µl Lipofectamine 2000 (Invitrogen, 11668019) according to the manufacturer's instructions. After a 48-h recovery, cells were passaged to a 10-cm dish with same medium as before with the substitution of zeocin for 100 µg ml^{-1} hygromycin (Gibco, 10687-010) for the selection of cells that integrated the TDP-43-HA encoding sequence in the genome. Cells were selected for 2–3 weeks before expansion and banking, and afterwards cultured in the same medium.

For production of SarkoSpin-insoluble phosphorylated GFP-TDP-43 aggregates, 2×10^6 motor neuron–like mouse NSC-34 cells were plated on a Matrigel-coated (Corning, 354234) 10 cm dish in differentiation medium consisting of DMEM/F-12 (Gibco, 21331-020) supplemented with 1× B27 supplement (Gibco, 17504-044), 1% GlutaMAX, 1× N2 supplement (Gibco, 175020-01) and 0.1× penicillin-streptomycin. After 48 h, cells were transfected with 5 µg of GFP-TDP-43-HA and 20 µl Lipofectamine 2000 according to the manufacturer's instructions.

Viability assay on HEK293 cells. To study the toxicity of the SarkoSpin-insoluble pellets, 6×10^4 HEK293 cells per well were plated on a Matrigel-coated 24-well plate and TDP-43-HA expression was induced after 24 h with 1 µg ml^{-1} of doxycycline. At 20 h later, cells were mitotically arrested with 10 µM AraC (Sigma, C1768), and after another 6–8 h, they were transfected with freshly prepared SarkoSpin pellet fractions. To prepare the inocula, SarkoSpin pellets were washed with 300 µl of sterile PBS to remove traces of sarkosyl and remove the vast majority of lipid contaminants. Pellets were subsequently resuspended in 200 µl cell-culture-grade PBS and sonicated at 60% amplitude for 2 min of sonication time (1 s–on, 1 s–off pulses) in water-bath sonicator (Q500, QSonica). Sonicated material (20 µl) was transfected with 2.5 µl Lipofectamine in a total volume of 290 µl OptiMEM per well. An additional 210 µl of medium was added 4 h after protein transfection, followed by whole medium change after 24 h, with fresh doxycycline and AraC. For the viability measurements, on day 3 after lipofection, 55 µl of 5 mg ml^{-1} thiazolyl blue tetrazolium bromide (Sigma, D5655) was added per well and plates were incubated at 37 °C for 1 h. The reaction was stopped and the formazan solubilized with 100 µl of a solution containing 16% SDS, 40% dimethylformamide and 2% glacial acetic acid. Absorption of the solubilized formazan at 570 nm was subtracted from the absorption of cell debris and other contaminants at 630 nm. The values of absorption in cells expressing TDP-43-HA were divided by the those of noninduced cells, and the value of the ratio of cells inoculated with SarkoSpin pellets from control subjects was set to one by dividing every value by the average ratio of all control conditions. Every condition was performed in triplicate.

Immunocytochemistry. TDP-43-HA-expressing HEK293 cells on 24-well microscopy plates (Ibidi, 82406) inoculated with GFP-TDP-43-HA aggregates were washed once with PBS before fixation in 4% formaldehyde (Sigma) for 10 min at room temperature. After being washed twice with PBS, cells were permeabilized and blocked in blocking buffer (10% donkey serum (Millipore) with 0.3% Triton X-100 (Sigma) in PBS) for at least 30 min at room temperature. Primary antibodies to HA tag (1:500, Cell Signaling Technology) and GFP (1:1,000, Rockland Immunochemicals) were incubated in blocking buffer overnight at 4 °C. After three washes with PBS, secondary antibody Alexa-647 donkey anti-rabbit (Invitrogen, A-31573) was applied in PBS for 1 h at room temperature, followed by three additional washes in PBS. Cells were covered with coverslips using ProLong Gold Antifade Mountant with 4,6-diamidino-2-phenylindole (DAPI; Invitrogen, P36931).

Primary mouse cortical neuronal culture in 96-well plate. Timed pregnant C57/BL6J female mice were received from Charles River Labs at 2 days before initiation of the primary culture. Cortices were harvested from E18 (mouse embryonic day 18 of development) mouse embryos and dissociated enzymatically and mechanically (using the neuronal tissue dissociation kit, C-Tubes, and an Octodissociator with heaters, Miltenyi Biotech) to yield a homogenous cell suspension. The cells were then plated at 20,000 per well in 96-well plates in neuronal medium (Neuronal Macs medium, Miltenyi Biotech) containing 0.5% penicillin-streptomycin, 0.5 mM alanyl-glutamine and 2% Neurobrew supplement (Miltenyi Biotech). In such cultures, and in control conditions, neurons represented about 85–95% of the cell population, with astrocytes and oligodendrocytes reaching 5–15% ($GFAP^+$ or $CNPase^+$), whereas the microglia ($Iba1^+$) were undetectable (not shown). Thus, in the text, and for the sake of simplicity, they are referred to as "neurons." After 4 DIV, Sarkospin pellet pools from three control, three FTLD-TDP-A or three FTLD-TDP-C subjects were resuspended in sterile PBS and sonicated with a cup horn sonicator (Q500, QSonica) at 100% set amplitude for 4 min of 1 s pulse and 1 s pause, and added to the medium at four different dilutions after normalization based on BCA-measured (BiCinchoninic Acid assay) protein concentrations (1, 0.3, 0.1 and 0.03 µg of total protein amount). For controlling total protein amounts as well as levels of TDP-43 and pTDP-43 in the inocula, all treatment media were submitted to dot blotting with antibodies to actin, TDP-43 and pTDP-43.

High content imaging of neurite outgrowth. Neuritic network development was followed by phase contrast[39]. The signal was acquired using an Incucyte S3

platform (Essen Biosciences) with a 20× objective. White light was used for phase contrast, and green and red light-emitting diodes were used for fluorescence. Neurite outgrowth was computed from both the phase contrast (time lapse) and fluorescence images (endpoint) using Neurotrack software (Essen Biosciences). At 4 DIV, cultures were challenged with the four concentrations of SarkoSpin pellets or medium for untreated wells. At 6 days after inoculations, effects of the treatments were evaluated by live-cell staining with calcein-AM to visualize the viable neurons and their processes.

Randomization. Data collection was randomized as control and disease subject samples were assigned randomly to experimental procedures. We also ensured that all sample groups were included in each experiment to exclude any experiment- or experimenter-based biases. Similarly, in all SarkoSpin, mass spectrometry, ultracentrifugation, immunolabeling and microscopy procedures, all TDP-43 proteinopathy samples were randomized with control samples.

Blinding. Data collection and analysis were not performed blind to the conditions of the experiments, as they did not include any subjective measurement or incomplete data collection.

Statistical analysis. No statistical methods were used to predetermine sample sizes but we used the maximum number of samples that were available to us. When stated, normality of the data sets was verified with Shapiro-Wilk normality test and equality of variances with an F test. Otherwise, data distribution was assumed to be normal but this was not formally tested. We used *t*-tests for two-sample comparisons and one-way or two-way ANOVA followed by Tukey's multiple-comparison tests for more than two samples. Statistical analyses were performed with GraphPad Prism 7 software.

Compliance with ethical regulations for animal procedures. All experiments using mice and mouse embryos were carried out in accordance with the European Communities Council Directive 2010/63/EU on the care of animals used in scientific research and with approval by the ethics committee of the University of Bordeaux (C2A50).

Reporting Summary. Further information on research design is available in the Nature Research Reporting Summary linked to this article.

Data availability

Mass spectrometry raw files were uploaded to the ProteomeXchange Consortium via the PRIDE partner repository. Data set identifier: PXD007873. The data that support the findings of this study are available from the corresponding author upon request.

References

46. Leek, J. T., Johnson, W. E., Parker, H. S., Jaffe, A. E. & Storey, J. D. The sva package for removing batch effects and other unwanted variation in high-throughput experiments. *Bioinformatics* **28**, 882–883 (2012).
47. Ling, S. C. et al. ALS-associated mutations in TDP-43 increase its stability and promote TDP-43 complexes with FUS/TLS. *Proc. Natl Acad. Sci. USA* **107**, 13318–13323 (2010).

nature research

Corresponding author(s): Magdalini Polymenidou

Reporting Summary

Nature Research wishes to improve the reproducibility of the work that we publish. This form provides structure for consistency and transparency in reporting. For further information on Nature Research policies, see Authors & Referees and the Editorial Policy Checklist.

Statistical parameters

When statistical analyses are reported, confirm that the following items are present in the relevant location (e.g. figure legend, table legend, main text, or Methods section).

n/a	Confirmed	
☐	☒	The exact sample size (*n*) for each experimental group/condition, given as a discrete number and unit of measurement
☐	☒	An indication of whether measurements were taken from distinct samples or whether the same sample was measured repeatedly
☐	☒	The statistical test(s) used AND whether they are one- or two-sided *Only common tests should be described solely by name; describe more complex techniques in the Methods section.*
☐	☒	A description of all covariates tested
☐	☒	A description of any assumptions or corrections, such as tests of normality and adjustment for multiple comparisons
☐	☒	A full description of the statistics including central tendency (e.g. means) or other basic estimates (e.g. regression coefficient) AND variation (e.g. standard deviation) or associated estimates of uncertainty (e.g. confidence intervals)
☐	☒	For null hypothesis testing, the test statistic (e.g. *F*, *t*, *r*) with confidence intervals, effect sizes, degrees of freedom and *P* value noted *Give P values as exact values whenever suitable.*
☒	☐	For Bayesian analysis, information on the choice of priors and Markov chain Monte Carlo settings
☒	☐	For hierarchical and complex designs, identification of the appropriate level for tests and full reporting of outcomes
☐	☒	Estimates of effect sizes (e.g. Cohen's *d*, Pearson's *r*), indicating how they were calculated
☐	☒	Clearly defined error bars *State explicitly what error bars represent (e.g. SD, SE, CI)*

Our web collection on statistics for biologists may be useful.

Software and code

Policy information about availability of computer code

Data collection	Immunoblot chemiluminescence : ImageQuant LAS 4000 (GE Healthcare) Mass spectrometry: ProteinPilot v5.0 (Sciex); Proteome Discoverer 1.4 (Thermo Scientific) Microscopy and Immunofluorescence: Leica Advanced Fluorescence (Leica Microsystems); IncuCyte S3 Software v2018A (Essen Bioscience)
Data analysis	Statistics: Prism 7.0 (GraphPad) Immunoblot: Image Studio Lite 4.0.21 (LI-COR), ImageJ 1.51h (NIH) Mass spectrometry: ComBat 3.0 (GenePattern); Bioconductor v 3.7; R v 3.5.0 Microscopy and Immunofluorescence: FIJI 2.0.0 (ImageJ); Neurotrack module of IncuCyte S3 Software v2018A (Essen Bioscience)

For manuscripts utilizing custom algorithms or software that are central to the research but not yet described in published literature, software must be made available to editors/reviewers upon request. We strongly encourage code deposition in a community repository (e.g. GitHub). See the Nature Research guidelines for submitting code & software for further information.

Data

Policy information about availability of data

All manuscripts must include a data availability statement. This statement should provide the following information, where applicable:

- Accession codes, unique identifiers, or web links for publicly available datasets
- A list of figures that have associated raw data
- A description of any restrictions on data availability

Mass spectrometry raw datasets were uploaded to the ProteomeXchange Consortium via the PRIDE partner repository. Dataset identifier: PXD007873.
Data availability : The data that support the findings of this study are available from the corresponding author upon request (postmortem human brain samples used in this study are unique biological samples and are therefore not available on request, but similar samples – disease, brain region, age, gender – can be obtained upon adequate request to any official brain bank.

Field-specific reporting

Please select the best fit for your research. If you are not sure, read the appropriate sections before making your selection.

☒ Life sciences ☐ Behavioural & social sciences ☐ Ecological, evolutionary & environmental sciences

For a reference copy of the document with all sections, see nature.com/authors/policies/ReportingSummary-flat.pdf

Life sciences study design

All studies must disclose on these points even when the disclosure is negative.

Sample size	No statistical methods were used to pre-determine sample sizes but our sample sizes are similar to those reported in previous publications cited in main text.
Data exclusions	No data were excluded from our analysis.
Replication	All experiments represented in the study were repeated as mentioned in Methods section and figure legends. Immunoblots and ultracentrifugation gradient replication consisted of an experimentally independent repetition with same biological samples, as well as performing the same experiment with all biologically independent samples indicated. TEM, IHC, and IF replication consisted on performing the same experiment with biologically independent samples from the same group (control or disease). Cell inoculations replication consisted of an experimentally independent repetition with same biological samples, as well as performing the same experiment with all biologically independent samples indicated. All attempts for replication were successful. Patient variability is detailed in our manuscript.
Randomization	Patient samples were classified into disease subtypes, based on the clinical, genetic and neuropathological analysis done at the respective site, where the autopsies were performed. Data collection was randomized as control / disease patient samples were assigned randomly to experimental procedures. We also ensured that all different sample groups were included in each experiment to exclude any experiment / experimenter biases. Similarly, in all SarkoSpin, mass spectrometry, ultracentrifugation, immunolabelling and microscopy procedures, all TDP-43 proteinopathies samples were randomized with control samples.
Blinding	Data collection and analysis were not performed blind to the conditions of the experiments as they did not include any subjective measurement or incomplete data collection.

Reporting for specific materials, systems and methods

Materials & experimental systems

n/a	Involved in the study
☐	☒ Unique biological materials
☐	☒ Antibodies
☐	☒ Eukaryotic cell lines
☒	☐ Palaeontology
☐	☒ Animals and other organisms
☐	☒ Human research participants

Methods

n/a	Involved in the study
☒	☐ ChIP-seq
☒	☐ Flow cytometry
☒	☐ MRI-based neuroimaging

Unique biological materials

Policy information about availability of materials

Obtaining unique materials

The data that support the findings of this study are available from the corresponding author upon request (postmortem human brain samples used in this study are unique biological samples and are therefore not available on request, but similar samples – disease, brain region, age, gender – can be obtained upon adequate request to any official brain bank.
All information is included in Supplementary Table 1:
21 control, 16 ALS and FTD-ALS, 25 FTD-A, 3 FTD-B, 11 FTD-C, 3 FTD-Tau and 3 AD patient frozen samples of motor cortex, frontal cortex or precentral gyrus were obtained from the indicated brain banks.

Antibodies

Antibodies used

Primary antibody Name; Company; Cat.No; Dilution for IF; Dilution for WB
pTDP-43 pS409/410 Cosmobio CAC-TIP-PTD-M01 n/a 1:2000
pTDP-43 pS403/404 Cosmobio CAC-TIP-PTD-P05 1:500 n/a
TDP-43 human specific ProteinTech 60019-2-Ig n/a 1:5000
TDP-43 Novus Biologicals NBP1-92695 n/a 1:1000
TDP-43 ProteinTech 10782-2-AP n/a 1:2000
TDP-43 ProteinTech 18280-1-AP n/a 1:2000
hnRNP A1 Abcam ab5832 n/a 1:2000
hnRNP H Abcam ab10374 n/a 1:10000
FUS Bethyl Laboratories A300-293A n/a 1:10000
SOD1 Enzo Life Sciences ADI-SOD-100-F n/a 1:5000
Histone H3 Abcam ab1791 n/a 1:5000
Actin Sigma-Aldrich A5441 n/a 1:5000
PDHA1 Sigma HPA063053 1:500 n/a
OGDHL Thermo Scientific PA5-62626 1:750 1:1000
FBXO2 Thermo Scientific PA5-21619 1:100 n/a
GLO1 Abcam ab171121 1:5000 n/a
MYH10 Abcam ab204544 1:200 n/a
MYH10 Abcam ab684 n/a 1:2000
KBTBD11 Abcam ab169551 1:2000 1:1000
ASAH1 Sigma HPA005468 1:750 1:125
ALDH9A1 Abcam ab224360 1:200 n/a
DNAJC5 Sigma HPA012737 1:100 n/a
DNAJC5 Abcam ab89236 n/a 1:500
CTTN Thermo Scientific PA5-27134 1:100 n/a
TXNL1 Sigma HPA002828 1:50 n/a
TXNL1 Abcam ab188328 n/a 1:1000
PITHD1 Sigma HPA016936 1:200 n/a
HPRT1 Thermo Scientific PA5-22281 1:250 n/a
HnRNP A1 Sigma HPA001609 1:350 n/a
CAPZB Abcam ab175212 1:250 n/a
HIST2H3PS2 Sigma HPA042570 1:100 n/a
Ubiquitin Millipore 05-1307 n/a 1:1000
PFN1 Sigma P7624 n/a 1:1000
PLIN4 Proteintech 55404-1-AP n/a 1:1000
IDH1 Proteintech 66197-1-Ig n/a 1:1000
LAMA1 Novus Biologicals CL3087 n/a 1:700
GAPDH Abcam ab8245 n/a 1:5000

Secondary antibody Name; Company; Cat.No; Dilution for IF; Dilution for WB
Donkey anti-mouse 488 Life Technologies A-21202 1:500 n/a
Donkey anti-mouse 594 Life Technologies A-21203 1:500 n/a
Donkey anti-mouse 546 Life Technologies A-10036 1:500 n/a
Donkey anti-mouse 647 Life Technologies A-31571 1:500 n/a
Donkey anti-rabbit 488 Life Technologies A-21206 1:500 n/a
Donkey anti-rabbit 546 Life Technologies A-10040 1:500 n/a
Donkey anti-rabbit 594 Life Technologies A-21207 1:500 n/a
Donkey anti-rabbit 647 Life Technologies A-31573 1:500 n/a
Goat anti-mouse HRP Jackson Immuno Research 115-035-146 n/a 1:10000
Goat anti-rabbit HRP Jackson Immuno Research 111-035-144 n/a 1:10000

Validation

Each antibody was validated for the respective species (human, mouse) and application (WB, DB, IF, IHC, EM) by the correspondent manufacturer, and is publicly available on its website with indicated catalogue numbers.

Eukaryotic cell lines

Policy information about cell lines

Cell line source(s)	Flp-In™ T-REx™ 293 (Invitrogen, R78007) NSC-34 (Bioconcept, CLU140)
Authentication	None of the cell lines have been authenticated.
Mycoplasma contamination	All cell lines were tested negative for mycoplasma contamination.
Commonly misidentified lines (See ICLAC register)	No commonly misidentified lines were used.

Animals and other organisms

Policy information about studies involving animals; ARRIVE guidelines recommended for reporting animal research

Laboratory animals	Two 2.5 months-old timed pregnant C57/BL6J female mice were received from Charles River Labs and E18 mouse embryos cortices were harvested for the primary neuronal cultures.
Wild animals	No wild animals were used.
Field-collected samples	No field-collected samples were used.

Human research participants

Policy information about studies involving human research participants

Population characteristics	All human specimens mentioned in this study are human brain autopsy material.
Recruitment	All patient material has been collected from donors for or from whom a written informed consent for a brain autopsy and the use of the material and clinical information for research purposes has been obtained by the respective institution.